Carbon Dioxide Capture Using Solid Sorbents in a Fluidized Bed with Reduced Pressure Regeneration in a Downer

Sunti Kongkitisupchai and Dimitri Gidaspow
Dept. of Chemical and Biological Engineering, Illinois Institute of Technology, Chicago, IL 60616

DOI 10.1002/aic.14215
Published online September 6, 2013 in Wiley Online Library (wileyonlinelibrary.com)

The most common technology for postcombustion CO_2 capture for existing power plants is the amine solvent scrubber. The energy consumption for capturing CO_2 from flue gases using amine solvent technology is 15 to 30% of the power plant electricity production. Hence, there is a need to develop more efficient methods of removing CO_2. Here, we show a novel design, obtained using multiphase CFD, and of a fluidized-bed reduced pressure regenerator, coupled with a fluidized-bed sorber, which has the potential to reduce the energy consumption. The undesirable core-annular flow regime in the riser-sorber is eliminated using multiple jet inlets and large particles leading to a shorter height. Up to 88% of the heat liberated in the riser-sorber is recovered in the downer-regenerator. © 2013 American Institute of Chemical Engineers *AIChE J*, 59: 4519–4537, 2013

Keywords: fluidization, computational fluid dynamics, energy, gas purification, multiphase flow

Introduction

The majority of the power plants in the United States use fossil fuel as the main source of energy. Coal-fired power plants generate approximately 40% of the electricity in the United States.[1] Department of Energy, Energy Information Agency (EIA), projects that electricity generated from coal-fired power plant will be increased from current capacity of 300 GW to nearly 450 GW by the year 2030.[2]

According to EIA estimates, fossil fuels accounted for over 40% of 5.8 billion metric tons of greenhouse gases, such as carbon dioxide (CO_2) in 2008.[3] Carbon dioxide (CO_2) emissions allowance credits were traded approximately 60 billion dollars in Europe and Japan, where governments regulate greenhouse gases.[4] Coal-fired power plants are continuously making progress in reducing emissions of nitrogen oxide, sulfur dioxide, particulate matter and mercury. However, reducing CO_2 emission from the flue gas with minimal energy consumption is still continuing to be a challenge. Currently, there are four main approaches for capturing the CO_2 generated from the power plants that use fossil fuel as primary energy sources[3] (1) precombustion CO_2 capture process, (2) postcombustion CO_2 capture systems, (3) oxycombustion CO_2 capture systems, and (4) chemical looping systems.

The energy consumption for capturing CO_2 from flue gases using amine solvent technology is 15 to 30% of the power plant.[5–7] The minimum energy for separation of CO_2 from flue gases, 7.3 kJ/g mol-CO_2, is already about one-third of the energy required for separation using aqueous amines.[7–9] There is little room for improvement using conventional solvent technology. The size of the amine scrubber unit is fairly large. For example, in a conventional coal fired power of 329 MWe plant,[5] there will be four absorber columns, 8.8 m in diameter and 24 m high. The stripper will have a diameter of 4.9 m and a height of 22.9 m. The steam requirement is 552 million kg/h at 0.3 MPa.

The objective of this study is to demonstrate the design of a complete loop system for dry solid sorbent technology for capturing CO_2 from conventional coal-fired power plant flue gases using the recently developed kinetic theory based multiphase computational fluid dynamics (CFD). The complete loop system consists of an atmospheric fluidized-bed riser-sorber and a reduced pressure downer-regenerator. The solid sorbents capture CO_2 and water from flue gases through chemical sorption in the sorber-riser. The captured CO_2 is released from the sorbent along with water in the reduced pressure regenerator-downer. The system should demonstrate the possibility of solving three main technical challenges which are the handling of large volumetric flow rate of the flue gases, the required operating power, and the quantity of CO_2 sorption. RTI (Nelson et al.[11–13]) developed some of this technology and manufactured 75 micron sodium carbonate pellets.

System Details and Descriptions

Process descriptions

The innovative compact sorption-riser and regeneration-downer system is shown in Figure 1. The dry solid sorbent system is selected because it is suitable to integrate into the existing power plants for postcombustion CO_2 capture when the CO_2 concentration in the flue gas is medium or low. Additionally, the sorption-riser and regeneration-downer system can handle large volumetric flow rates of flue gases and requires low energy to regenerate the sorbent, which are the

Correspondence concerning this article should be addressed to S. Kongkitisupchai at skongkit@iit.edu.

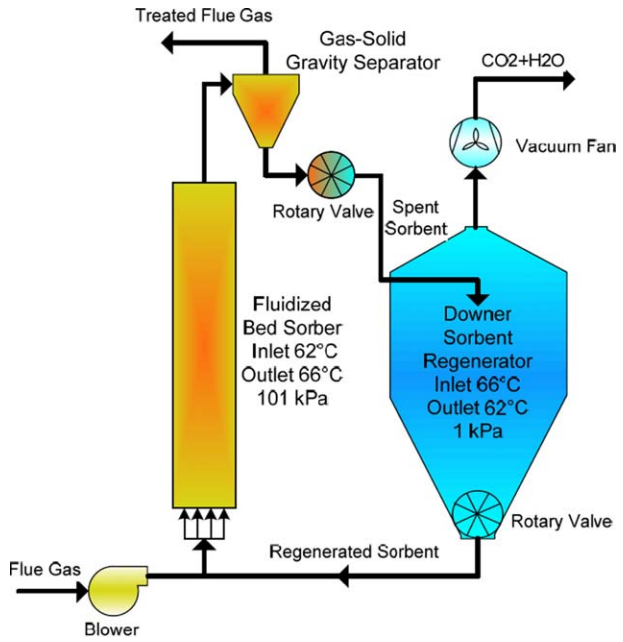

Figure 1. Carbon dioxide capture system with reduced pressure regeneration based on CFD design.

[Color figure can be viewed in the online issue, which is available at wileyonlinelibrary.com.]

key technical challenges to overcome in postcombustion CO_2 capture. The system comprises of the sorption-riser section and regeneration-downer section. The untreated flue gases flow into the system via the jet inlet at the bottom of the sorber-riser section which is called a sorption zone. This is the section where CO_2 and water vapor in the flue gases are sorbed into the solid sorbents. The CO_2 sorption occurs due to the fact that the partial pressure of the CO_2 in the untreated flue gases is higher than the equilibrium pressure of the CO_2 and sodium carbonate shift at the operating temperature. The treated flue gases leave the sorber-riser through the gas–solid gravity separator where the absorbed solid sorbents separate from the treated flue gases. The treated flue gases are released to the atmosphere, while the absorbed solid sorbents in the separator are gravity fed through the airlock-rotary valve down to regenerator-downcomer section for regeneration, which is called a desorption zone. The regenerator-downer section operates under reduced pressure environment where the CO_2 and water vapor can be easily desorbed from solid absorbents. The desorption of CO_2 and water vapor occurred inside the reduced pressure regenerator-downer because the partial pressure of CO_2 in the gases is lower than CO_2 equilibrium pressure at the downer operating temperature. The desorbed gases from solid sorbent in the desorption zone mainly consist of CO_2 and water vapor. The desorbed gases leave the downer-regenerator from the top opening above the solid inlet. In the cooler, the water vapor is separated from CO_2 by a conventional cooling process before the gas stream passes through a vacuum fan. The regenerated solid sorbents are sent back to the riser inlet section via a lock-hopper rotary valve, and again continue the sorption-regeneration cycle. Additionally, there are small amounts of CO_2 fed to the bottom of the regenerator-downer at minimum fluidization velocity which assist the circulation flow of solid sorbents. Such aeration is commonly used in fluidized bed technology.

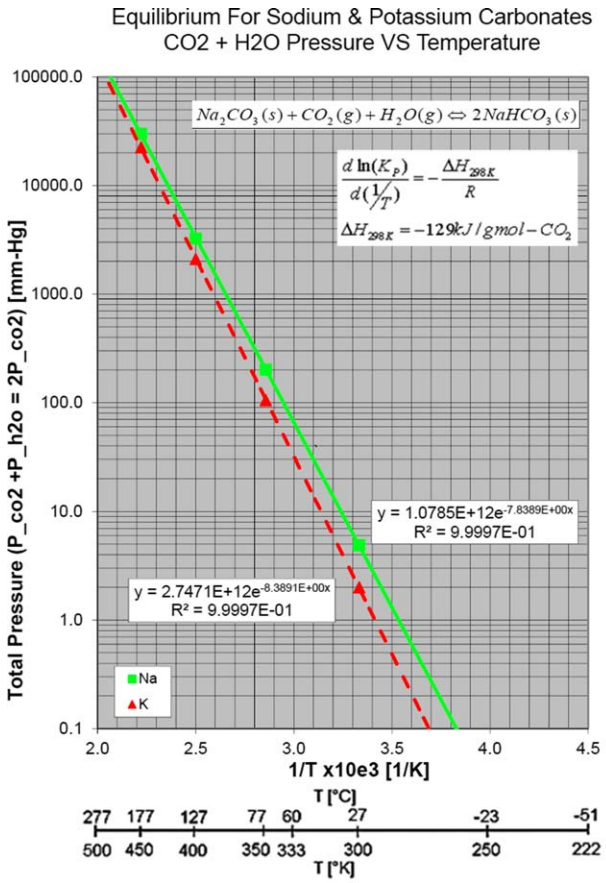

Figure 2. Temperature and partial pressure equilibrium curve for Sodium Carbonate/Bicarbonate.

[Color figure can be viewed in the online issue, which is available at wileyonlinelibrary.com.]

The equilibrium curve of the sodium carbonate and sodium bicarbonate system is shown in Figure 2. The equilibrium curve shows that the pressure of CO_2 and H_2O is quite sensitive to the temperature. As a result, a small change in the temperature can drastically affect the sorption or desorption capacity of the sodium-based solid sorbent. Figure 3 shows the full operating cycle of the system. It shows that the partial pressure of CO_2 and water vapor at

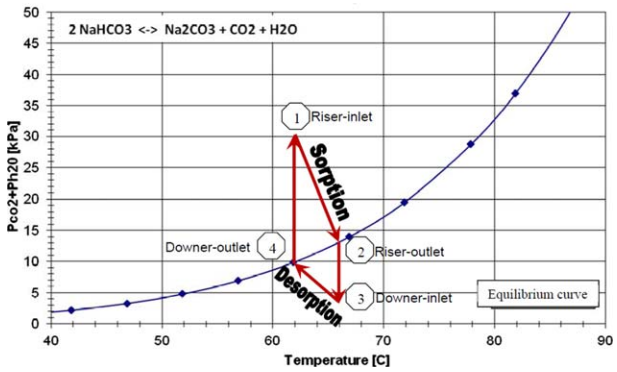

Figure 3. Sorber—regenerator CO_2 capture fluidized bed process.

Temperature and partial pressure equilibrium curve for sodium carbonate/bicarbonate. [Color figure can be viewed in the online issue, which is available at wileyonlinelibrary.com.]

the operating point#1 (sorber-riser inlet) is higher than the equilibrium pressure. Thus, the CO_2 and water will be sorbed by the solid sorbents. The CO_2 sorption process stops once the CO_2 partial pressure reaches the equilibrium line at the outlet of the sorber-riser (operating point#2). The operating point#3 is where the solid sorbent is fed into the regenerator-downer from the gas–solid gravity separator via a rotary lock-hoper valve. The CO_2 desorption occurs in the regenerator-downer, which operates under reduced pressure. Under the reduced pressure operating condition, the partial pressure of CO_2 and water vapor is lower than equilibrium pressure causing the CO_2 and water vapor to desorb from the solid sorbent. Once the pressure equilibrium is reached at the bottom of the regenerator-downer, the CO_2 desorption process is stopped. This is operating point#4 in Figure 3.

Figures 2 and 3 shows that the operating temperature is one of the important parameters for the dry solid sodium-based sorbent CO_2 capture system. Low gas and solid temperatures make CO_2 sorption faster and easier because the CO_2 equilibrium pressure is low. However, low temperatures make CO_2 desorption more difficult or nearly impossible due to the low-equilibrium pressure. Thus, the operating pressure in the regenerator-downer needs to be low. At higher gas and solid temperatures, the CO_2 sorption is more difficult due to the high CO_2 equilibrium pressure. On the other hand, high temperature makes CO_2 desorption easy due to the high CO_2 equilibrium pressure compared to operating pressure. The operating temperatures in the sorber-riser and regenerator-downer must be selected carefully to maximize the system performance and minimize the energy consumption.

The untreated flue gases enter the sorber at 55°C and exit at 66°C while the solid sorbents enter the sorber at 62°C and exit at 66°C. Almost all heat of reaction liberated in sorption zone in the riser is captured in the solid sorbent. Due to the high-circulation rates, the temperature of the solid sorbent rises only at 4°C. This is similar to the study of Chalermsinsuwan et al.[14] This small rise in the solid and gas temperatures keeps the sorption capacity of the solid sorbent relatively constant. The heat of reaction captured in the solid sorbent from the sorber-riser is recovered in the regenerator-downer. The solid sorbents enter the regenerator-downer at 66°C. The solid sorbent regeneration is an endothermic reaction. The heat captured in the solid sorbent from the sorption step is used as the energy in the regeneration step. The solid sorbents leave the regenerator-downer at 62°C and are ready for circulation in the sorber-riser.

Based on our CFD calculation we projected the parasitic energy consumption for the flue gas blower in Figure 1 to be about 4.2 kJ/g-mol CO_2 vs. 372 kJ/g-mol CO_2 for carbon combustion. The energy consumption for the vacuum fan is 23.4 kJ/g-mol CO_2. It supplies the required minimum energy of separation of 7.3 kJ/g-mol CO_2. The work required for two airlock rotary valves require approximately 0.7 kJ/g-mol CO_2 each.

The aforementioned estimate of parasitic electricity losses has been verified by a thermodynamic availability analysis shown later in the thermodynamic section. In the riser-sorber, there is an availability gain of 7.9 kJ/g-mol CO_2 due to a small rise in temperature. This availability gain is almost all recovered in the regeneration step in the downer. The availability loss in the downer is 36.9 kJ/g-mol CO_2. Therefore, the net availability of 29.0 kJ/g-mol CO_2 is supplied by the work from the downer vacuum fan, the riser blower, and other accessory instruments such as airlock rotary valves. In the alternate concept, if the carbon dioxide were absorbed in a bubbling bed with cooling, the availability loss in the bubbling bed sorber would be 7.9 kJ/g-mol CO_2 due to loss of energy to cooling media.

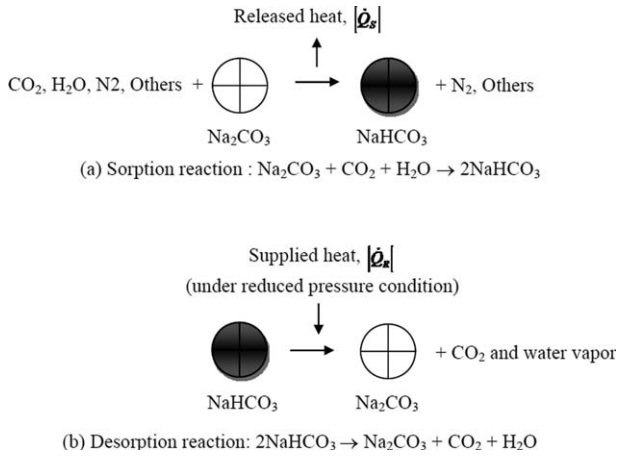

Figure 4. Block diagrams of (a) sorption reaction, and (b) desorption reaction.

Solid sorbent descriptions

The sorption and desorption reactions between the solid sorbent CO_2, and water vapor are shown in Figure 4 as a block diagram. The sorption reaction occurs at sorption temperature T_S, while the regeneration reaction occurs at regeneration temperature T_R. The CO_2 sorption reaction is an exothermic reaction while desorption reaction is an endothermic reaction. The heat of reaction $\dot{Q}_S$, liberated in the sorption zone equals to the total amount of enthalpy change in gas and solid phases. The change in enthalpies of gas and solid sorbent is in form of the temperature rise. The entropy rise in the gas phase considers as an irreversibility of the system because the energy increase in the gas phase cannot be recovered in the regenerator-downer. The required power for regeneration reaction, which is an endothermic reaction, comes from the energy captured in the solid sorbent and the energy used to generate the vacuum. The overall Na_2CO_3 solid sorbent reaction is

$$\begin{aligned} &Na_2CO_3 + CO_2 + H_2O <=> 2\ NaHCO_3 \\ &\Delta H_{298K} = -129.16 kj/g - \text{mol}\, CO_2 \end{aligned} \tag{1}$$

The selection of the solid sorbent has a significant impact on the unit performance and energy consumption which are the two major technical challenges of this system. The energy requirement topic is a main issue for this article. Chalermsinsuwan et al.[14] showed that the system performance decreases with increasing operating temperature difference between sorber-riser and regenerator-downer. Additionally, the smaller the difference of temperature, the smaller the minimum required power for regeneration process.

There are many alkali and alkali-earth base dry solid sorbent available for CO_2 sorption which have been reported in many articles.[14–20] In this study, the alkali-based sodium carbonate (Na_2CO_3) is chosen as the solid sorbent because its CO_2 sorption capacity is high and its required vacuum pressure for regeneration at low temperature is reasonable.[17] Additionally, the sodium carbonate (Na_2CO_3) is nontoxic, low cost and fairly easy to obtain. Table 1[14] summarizes the

Table 1. The Heat Regenerative Reaction for Various Preparations of Alkaline Carbonates
$2MHCO_3 \rightarrow M_2CO_3 + CO_2 + H_2O$
(M = metal of an alkaline)

Compound	Heat of regenerative reaction (MJ/kgmol)
Li_2CO_3	48.61
Na_2CO_3	129.16
K_2CO_3	137.41
Rb_2CO_3	148.84
Cs_2CO_3	157.21

heat of regeneration reaction for various preparations of alkaline carbonates.

Although the required regeneration energy for sodium carbonate (Na_2CO_3) is higher than lithium carbonate (Li_2CO_3), the CO_2 sorption capacity of sodium carbonate Na_2CO_3 is more than lithium carbonate (Li_2CO_3). Other solid sorbents, such as for potassium carbonate (K_2CO_3), rubidium carbonate (Rb_2CO_3) or cesium carbonate (Cs_2CO_3) require a higher regeneration energy at the same operating temperatures as the sodium carbonate (Na_2CO_3). Rubidium carbonate (Rb_2CO_3) or cesium carbonate (Cs_2CO_3) are also expensive.

Fluidized-bed riser-sorber

The study of Chalermsinsuwan B et al.[14] showed that circulating fluidized beds (CFB) can be used effectively for CO2 sorption from the flue gases generated by conventional coal fired power plants. However, the solid flow patterns in the sorber section for the CFB showed some fluctuation of the gas and solid flows which allow some of the untreated flue gases to channel through the sorber section. The core-annular regime occurred in the sorber section. These problems can be almost completely eliminated by improving the inlet conditions and some solid sorbent properties. The recent study by Khongprom and Gidaspow[21] showed that a compact fluidized-bed riser sorber with a proper configuration can eliminate the usual core-annular flow in the circulating fluidized beds. The simulations in this study for the riser-sorber section were done similarly to the Khongprom and Gidaspow[21] study. However, there were some changes in some parameters in the simulations. Figure 5 and Table 2

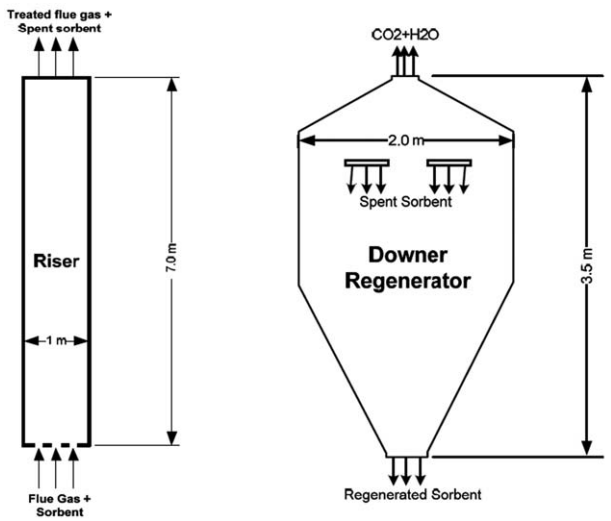

Figure 5. Riser-sorber and downer-regenerator simulation conditions.

Table 2. Parameters used for the Simulation

Symbol	Description	Value
ρ_g	Gas density	1.04 kg/m^3
μ_g	Gas viscosity	2×10^{-5} kg/m s
ρ_s	Solid sorbent density	500 kg/m^3
d_p	Solid sorbent diameter	500 μm
G_s	Solid sorbent circulation rate	48 kg/s
e	Restitution coefficient between particles	0.90
e_W	Restitution coefficient between particle and wall	0.80
ϕ	Specularity coefficient	0.10
T	Simulation time (minimum)	100 s
At the bottom of the riser section		
v_g	Inlet gas velocity	1 m/s
T_g	Inlet gas temperature	328.15 K
v_s	Inlet solid sorbent velocity	At solid circulation rate
T_s	Inlet solid sorbent temperature	From the downer outlet
$y_{Na_2CO_3}$	Inlet Na_2CO_3 species mole fraction	From the downer outlet
y_{NaHCO_3}	Inlet $NaHCO_3$ species mole fraction	From the downer outlet
y_{CO_2}	Inlet CO_2 species mole fraction	0.15
y_{H_2O}	Inlet water vapor species mole fraction	0.15
y_{inert}	Inlet non-reacted species mole fraction	0.70
ε_s	Solid volume fraction	0.15
At the top of the downcomer section		
v_s	Inlet solid sorbent velocity	At solid circulation rate
T_s	Inlet solid sorbent temperature	From the riser outlet
$y_{Na_2CO_3}$	Inlet Na_2CO_3 species mole fraction	From the riser outlet
y_{NaHCO_3}	Inlet $NaHCO_3$ species mole fraction	From the riser outlet
ε_s	Solid volume fraction	0.60

shows the simulation conditions, geometry and configuration of riser-sorber and downer-regenerator. The riser-sorber is a 1 m wide and 7 m high column. We have used the kinetic theory based CFD model in fluent to solve the conservation of mass, momentum, chemical species, and energy equations, with reaction kinetics shown in Table 3. The new proposed reaction rate is used in the riser simulation. The riser-sorber has four inlet jets at the bottom, where untreated flue gas and solid sorbent are fed into the column. The outlet of the riser-sorber column is straight open.

The mixture of untreated flue gases and solid sorbents enter the fluidized bed riser through a series of jets, as shown in Figure 5. The untreated flue gases from a power plant flow to the sorber-riser at 55°C, as shown in Figure 1. The 500 micron solid sorbents are supplied to the sorber-riser from the downer-regenerator via a rotary valve. The temperature of the solid sorbents entering the sorber-riser is the same as the solid sorbent at the bottom of the downer-regenerator, which is approximately 62°C. The inlet velocity of sorber-riser simulation is set at a constant feed gas velocity of 1.0 m/s and the solid flux of 48 kg/m^2/s. The sorber riser inlet solid volume fraction is 15%. The riser-sorber is operating at atmospheric pressure at the top outlet. The conditions of the solid sorbent at the outlet of the riser-sorber are used as the inlet conditions for the downer-regenerator.

Downer regenerator

Vacuum regeneration of sorbents is a common industrial operation. As the pressure is lowered, the regeneration temperature decreases. Hence, a lower level heat can be used for

Table 3. A Summary of the Governing Equations and Constitutive Equations[35,36]

A. Governing equations;

(a) Conservation of mass;

Gas phase;

$$\frac{\partial}{\partial t}\left(\varepsilon_g\rho_g\right)+\nabla\cdot\left(\varepsilon_g\rho_g v_g\right)=\dot{m}_g \tag{1}$$

Solid phase;

$$\frac{\partial}{\partial t}\left(\varepsilon_s\rho_s\right)+\nabla\cdot\left(\varepsilon_s\rho_s v_s\right)=\dot{m}_s \tag{2}$$

Where, $\dot{m}_s=-\dot{m}_g$ and $\dot{m}_g=\sum_j^N MW^j r^j$

(b) Conservation of momentum;

Gas phase;

$$\frac{\partial}{\partial t}\left(\varepsilon_g\rho_g v_g\right)+\nabla\cdot\left(\varepsilon_g\rho_g v_g v_g\right) =-\varepsilon_g\nabla P+\nabla\cdot\tau_g+\varepsilon_g\rho_g g-\beta_{gs}\left(v_g-v_s\right) \tag{3}$$

Solid phase;

$$\frac{\partial}{\partial t}\left(\varepsilon_s\rho_s v_s\right)+\nabla\cdot\left(\varepsilon_s\rho_s v_s v_s\right) =-\varepsilon_s\nabla P+\nabla\cdot\tau_s-\nabla P_s+\varepsilon_s\rho_s g+\beta_{gs}\left(v_g-v_s\right) \tag{4}$$

(c) Conservation of energy;

Gas phase;

$$\frac{\partial}{\partial t}\left(\varepsilon_g\rho_g H_g\right)+\nabla\cdot\left(\varepsilon_g\rho_g v_g H_g\right) =-\left(\frac{\partial P_g}{\partial t}+P_g\nabla\cdot v_g\right)+\tau_g:\nabla\cdot v_g+S_g+Q_{sg} \tag{5}$$

with

$$H_g=\int c_{p,g}dT_g,$$

Q_{sg} calculated based on Gunn's model as shown in Yuanxiang and Gidaspow[35]

Solid phase;

$$\frac{\partial}{\partial t}\left(\varepsilon_s\rho_s H_s\right)+\nabla\cdot\left(\varepsilon_s\rho_s v_s H_s\right)=\tau_s:\nabla\cdot v_s+S_s+Q_{gs} \tag{6}$$

with

$$H_s=\int c_{p,s}dT_s,$$

Q_{gs} calculated based on Gunn's model as shown in Yuanxiang and Gidaspow[35]

(d) Conservation of species ($j=CO_2$, H_2O, air (O_2+N_2) and $i=NaHCO_3$, and Na_2CO_3);

$$\frac{\partial}{\partial t}\left(\varepsilon_g\rho_g y_j\right)+\nabla\cdot\left(\varepsilon_g\rho_g v_g y_j\right)=\alpha_j MW_j r \tag{7a}$$

$$\frac{\partial}{\partial t}\left(\varepsilon_s\rho_s y_i\right)+\nabla\cdot\left(\varepsilon_s\rho_s v_s y_i\right)=\alpha_i MW_i r \tag{7b}$$

(e) Conservation of solid phase fluctuating energy;

$$\frac{3}{2}\left[\frac{\partial}{\partial t}\left(\varepsilon_s\rho_s\theta\right)+\nabla\cdot\left(\varepsilon_s\rho_s\theta\right)v_s\right] =\left(-\nabla p_s\bar{I}+\tau_s\right):\nabla v_s+\nabla\cdot\left(\kappa_s\nabla\theta\right)-\gamma_s \tag{8}$$

B. Constitutive equations;

(a) Gas phase stress;

$$\tau_g=\varepsilon_g\mu_g\left[\nabla v_g+\left(\nabla v_g\right)^T\right]-\frac{2}{3}\varepsilon_g\mu_g\left(\nabla\cdot v_g\right)I \tag{9}$$

(b) Solid phase stress;

$$\tau_s=\varepsilon_s\mu_s\left[\nabla v_s+\left(\nabla v_s\right)^T\right]-\varepsilon_s\left(\xi_s-\frac{2}{3}\mu_s\right)\nabla\cdot v_s I \tag{10}$$

Table 3. *Continued*

(c) Collisional dissipation of solid fluctuating energy;

$$\gamma_s=3\left(1-e^2\right)\varepsilon_s^2\rho_s g_0\theta\left(\frac{4}{d_p}\sqrt{\frac{\theta}{\pi}}\right) \tag{11}$$

(d) Radial distribution function;

$$g_0=\left[1-\left(\frac{\varepsilon_s}{\varepsilon_{s,\max}}\right)^{1/3}\right]^{-1} \tag{12}$$

(e) Solid phase pressure;

$$p_s=\varepsilon_s\rho_s\theta[1+2g_0\varepsilon_s(1+e)] \tag{13}$$

(f) Solid phase shear viscosity;

$$\mu_s=\frac{4}{5}\varepsilon_s\rho_s d_p g_0(1+e)\sqrt{\frac{\theta}{\pi}}+\frac{10\rho_s d_p\sqrt{\pi\theta}}{96(1+e)g_0\varepsilon_s}\left[1+\frac{4}{5}g_0\varepsilon_s(1+e)\right]^2 \tag{14}$$

(g) Solid phase bulk viscosity;

$$\xi_s=\frac{4}{3}\varepsilon_s\rho_s d_p g_0(1+e)\sqrt{\frac{\theta}{\pi}} \tag{15}$$

(h) Conductivity of the fluctuating energy;

$$\kappa_s=\frac{150\rho_s d_p\sqrt{\theta\pi}}{384(1+e)g_0}\left[1+\frac{6}{5}\varepsilon_s g_0(1+e)\right]^2 +2\rho_s\varepsilon_s^2 d_p(1+e)g_0\sqrt{\frac{\theta}{\pi}} \tag{16}$$

(i) Gas-solid phase interphase exchange coefficient;

when $\varepsilon_g\le 0.80$;

$$\beta_{gs}=150\frac{\left(1-\varepsilon_g\right)^2\mu_g}{\varepsilon_g d_p^2}+1.75\frac{\left(1-\varepsilon_g\right)\rho_g|v_g-v_s|}{d_p} \tag{17}$$

when $\varepsilon_g>0.80$;

$$\beta_{gs}=\frac{3}{4}\frac{\left(1-\varepsilon_g\right)\varepsilon_g}{d_p}\rho_g|v_g-v_s|C_{D0}\varepsilon_g^{-2.65} \tag{18}$$

with

$\mathrm{Re}_k<1000$; $C_{D0}=\frac{24}{\mathrm{Re}_k}\left(1+0.15\mathrm{Re}_k^{0.687}\right)$;

$\mathrm{Re}_k=\frac{\rho_g\varepsilon_g|v_g-v_s|d_p}{\mu_g}$

$\mathrm{Re}_k\ge 1000$; $C_{D0}=0.44$

(j) Reaction rate;

$$r=-k_{reaction}\left(C_{CO_2,eq}-C_{CO_2}\right)\left(C_{H_2O,eq}-C_{H_2O}\right) \tag{19}$$

where, $k_{reaction}=55.0\exp\left(\frac{3609}{RT}\right)$

$$C_{CO_2,eq}+C_{H_2O,eq}=\frac{P_{CO_2+H_2O,eq}}{RT}$$

A similar model for production of liquid fuels from synthesis gas was developed earlier by Yuanxiang and Gidaspow[35] and used by Gamwo, et al.[37] to obtain an optimum catalyst size.

regeneration. The vapor pressure data shows that at a temperature as low as 60° centigrade the vapor pressure of the sodium carbonate sorbents is high enough for vacuum regeneration. The equilibrium data for the reaction show that the pressure at 66°C is 13.5 kPa(abs). However, due to lack of information on chemical kinetic reaction model, the downer was selected to run at 1.0 kPa(abs) to ensure that the solid sorbent can be completely regenerated before leaving the

downer-regenerator. The downer is 2.0 m wide and 3.5 m tall vessel.

Figure 1 shows that the solid sorbent particles are fed into the downer-regenerator via an air-lock rotary valve. The downer-regenerator geometry and inlet conditions are shown in Table 2 and Figure 5. The spent solid sorbents are fed into the upper section of the regenerator-downer through the slots. The downer-regenerator is purposely designed to have the middle section larger than the inlet and outlet sections. This unique shape allows the gases desorbed from the solid sorbent during the regeneration process to expand which cause a reduction in the upward velocity. As a result, the solid sorbent can drop to the bottom section by gravity without getting carried over by the gases to the top outlet.

Regenerated sorbent particles are removed from the bottom of the downcomer-regenerator by gravity. The desorbed gases, which mostly consist of carbon dioxide and water vapor, exit at the top of the riser. Water vapor is removed in a cooler heat exchanger, while the carbon dioxide flows through a vacuum fan. The compressed carbon dioxide is ready for sequestration or for other applications. The solid sorbents enter the downer-regenerator through an airlock rotary valve which isolates the reduced pressure regenerator from the fluidized-bed sorber. At the top, the outlet pressure is maintained at 1 kPa(abs) by the vacuum fan as shown in Figure 1. The pressure at the bottom of the downer is approximately 3 kPa(abs) due to the weight of the solid sorbents. The solids are removed through the center rotary valve which increases the pressure from 3 kPa(abs) to 101 kPa(abs).

Computational Fluid Dynamics Simulation

Hydrodynamics model

A set of governing equations, mass, momentum, energy and component species mass conservation equations, as well as constitutive equations were solved numerically. The constitutive equations are based on the kinetic theory of granular flow, as reviewed by Gidaspow.[22] This theory has proved its validity by many researchers.[14,23,24] An additional custom chemical reaction equation was added as a port of constitutive equations. The commercial CFD program FLUENT 6.2.16 was chosen for modeling the system. The Eulerian-Eulerian model was selected for the simulations. A summary of the governing equations and constitutive equations is given in Table 3.

In this simulation, the riser-sorber and downer-regenerator were run separately. To ensure that the riser-downer loop system was at a steady-state. The following steps were strictly followed.

1. The riser-sorber simulation was run based on an estimate of initial conditions and fixed inlet conditions for gas and solid.
2. Once the riser-sorber reached the quasi-steady-state operation, the important time-averaged variables at the riser-sorber outlet were calculated.
3. The downer-regenerator simulation was run based on an estimate of initial conditions and inlet condition variables which were obtained from riser-sorber outlet by the time-averaged method in step 2.
4. The important time-averaged variables at the downer-regenerator outlet were obtained after the downer reached a quasi-steady-state operation.
5. The obtained time-averaged variables for solid sorbent from step 4 were used as the new inlet conditions of the riser-sorber simulation. The inlet conditions for flue gas remain unchanged.
6. Step 1 to step 5 were repeated until time-averaged variables at the outlet of both riser-sorber and downer-regenerator were unchanged from previous iteration.

The computational domains of the both riser and downer systems are illustrated in Figure 6a and 6b. The riser-sorber consists of 3,276 computational cells, while downer-regenerator consists of 8,064 computational cells. Both riser and downer were run using a time step of 0.001 s, with a maximum of 100 iterations per time step. Every simulation run for the riser-sorber and downer-regenerator reached a minimum of 100 s of flow time to ensure that a quasi-steady-state was reached. The models were solved using a standard desktop computer.

Chemical reaction model

An accurate reaction rate model for the Na_2CO_3 – CO_2 – $NaHCO_3$ is currently not available. Most of the researches focused only on the preparation, sorption characteristic, and sorption capacity of the sorbents. Additionally, most of the CO_2 sorption-desorption on solid sorbent studies focused on K_2CO_3 rather than Na_2CO_3. Onischak and Gidaspow[25] studied the feasibility of transferring CO_2 from the anode of a molten carbonate fuel cell to its cathode using solid K_2CO_3. They determined the rates of reaction in a parallel plate reactor as a function of CO_2 concentration and time in the range of 0.50–20.00% CO_2 and developed a reaction model. The pressure and temperature equilibrium data of various carbonates obtained by Gidaspow is shown in Figure 2. The

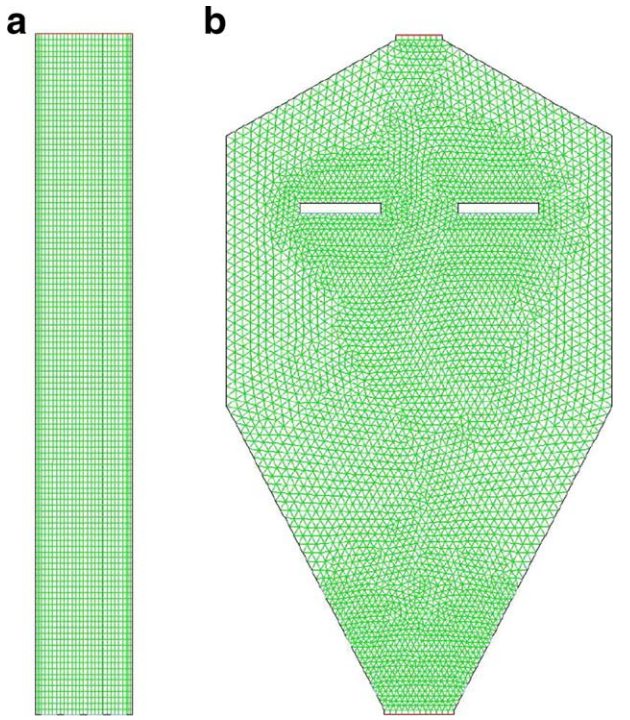

Figure 6. (a) Computational domain of the riser-sorber system. (b) Computational domain of the downer-regenerator system.

[Color figure can be viewed in the online issue, which is available at wileyonlinelibrary.com.]

equilibrium data was used to determine the CO_2 partial pressure equilibrium at operating temperature in the simulation. Although past research by Gidaspow[17,25] deals with the preparation of sorbent sheets for stationary sorbers, it should be possible to use a similar preparation method for making spherical pellets for use in fluidized beds. Lee et al.[26] did some study on different forms of Na_2CO_3, but there is no conclusion about the reaction rate. Charles[27] also studied the pressure-temperature relationship for decomposition of sodium bicarbonate from 200 to 600°F. However, there was no reaction rate mentioned. Additionally the temperature range is much higher than the operating temperature in the riser or downer in this simulation. Recently, Park et al.[28] measured the breakthrough data of CO_2 to obtain the kinetics of the CO_2-K_2CO_3 reaction using a shrinking-core model and a deactivation model. Moreover, Park et al.[24] and Yongwon Seo et al.[29,30] showed that the concentration of water vapor in the feed stream affects the sorption rate of CO_2 for Na_2CO_3 and K_2CO_3. Therefore, this study also assumes that water concentration in the flue gases affects the CO_2 sorption rate, similar to the CO_2.

Onischak and Gidaspow[25] showed that CO_2 sorption capacity of Na_2CO_3 solid sorbent is very sensitive to the temperature. Due to the lack of sorption-desorption rate data for the Na_2CO_3 solid sorbent, the sorption-regeneration loop system is based on the pressure equilibrium of CO_2-H_2O—Na_2CO_3-$NaHCO_3$. A new reaction rate is proposed. In order to simulate the novel sorption-regeneration system, this study used the sorption and desorption rate equation modified from Gidaspow[17,22] and Onischak and Gidaspow[25] study. The pressure equilibrium data and the equations can be found in Figure 2. The equilibrium pressure is converted to equilibrium concentration for CO_2 and water vapor, for proposed pressure based reaction model. The equation for temperature and pressure equilibrium for Na_2CO_3 is shown following

$$P_{CO_2+H_2O,eq}=1.0785\times10^{12}\left[\exp\left(\frac{-7.83893\times10^3}{T}\right)\right] \quad (2)$$

The proposed equation is a second-order reaction with respects to CO_2 concentration (C_{CO_2}) and H_2O concentration (C_{H_2O}), corrected for the decomposition pressure of the bicarbonate. The reaction rate equation (r) is shown below in terms of the driving forces for the reaction. This form allows a calculation of the rate of regeneration when the operating pressure is reduced below the decomposition pressure in terms of the measured forward rate constant $k_{reaction}$

$$r=-k_{reaction}\left(C_{CO_2,eq}-C_{CO_2}\right)\left(C_{H_2O,eq}-C_{H_2O}\right) \quad (3)$$

where, $k_{reaction}=55.0\exp\left(\frac{3609}{RT}\right)$ and where,

$$C_{CO_2,eq}+C_{H_2O,eq}=\frac{P_{CO_2+H_2O,eq}}{RT}$$

with the aforementioned decomposition pressure given by Eq. 2.

The proposed reaction rate (Eq. 3) is an extension of the sorption rate used by Chalermsinsuwan et al.[14] It is valid for small carbonate conversions, which occur at high-solid circulation rates used in this study. The proposed reaction rate allows a computation of reasonable desorption rates for regenerator studies. Initially, a mass-transfer coefficient reaction rate model was used to estimate rates of regeneration. The problem of using a mass transfer coefficient reaction rate model is that the mass coefficients in fluidized beds vary by several-orders of magnitude (Kashyap and Gidaspow[31]).

The commercial CFD code does not support the modeling of reaction rate for the heterogeneous phase system. The new additional UDF (user-defined function) code written in C programming language was added because the heterogeneous reaction rate equation is not available in the FLUENT 6.2.16 program.

Initial and boundary conditions

The simulation parameters at the inlet of riser-sorber and downer-regenerator, such as the flue gas velocity, solid-sorbent velocity, solid volume fractions, flue gas temperature, solid-sorbent temperature, and species composition for both gas and solid sorbent are summarized in Table 2. The operating pressure at the riser-sorber outlet was specified as atmospheric pressure. On the other hand, the operating pressure at the top outlet of the downer-regenerator was set at 1.0 kPa(abs). Initially, there were no Na_2CO_3 solid sorbents deposited inside the riser-sorber assumed to be zero at the initial start, while regenerator-downer sections were initially as set to have a solid sorbent deposit up to 2 m height, at 0.55 solid-volume fractions. The initially filled solid sorbents in the downer consisted of 100% of Na_2CO_3, which implied that fresh solid sorbents were used for the initial conditions. The initial velocities for both gas and solid sorbent in the riser-sorber were set at zero. Similarly, the gas and solid sorbent initial velocities in the downer-regenerator were set at zero.

The initial temperature in the riser-sorber was set to be uniform at 335 Kelvin (143.6°F). Additionally, the initial operating pressure inside the riser-sorber was set to be uniform at the atmospheric pressure (101.325 kPa). The initial temperature and operating pressure in the downer-regenerator were set to be homogeneous at 335 Kelvin (143.6°F) and 1.0 kPa(abs), respectively.

At the wall, a no-slip condition was applied for all velocities, except for the tangential velocity of the solid phase and the granular temperature. Here, the boundary conditions of Johnson and Jackson[32] were used. These conditions were first applied in the kinetic theory of granular flow modeling by Sinclair and Jackson.[33] They are

$$v_{st,W}=-\frac{6\mu_s\varepsilon_{s,max}}{\pi\phi\rho_s\varepsilon_s g_0\sqrt{3\theta}}\frac{\partial v_{st,W}}{\partial n} \quad (4)$$

$$\theta_W=-\frac{\kappa_s\theta}{\gamma_W}\frac{\partial\theta_W}{\partial n}+\frac{\sqrt{3}\pi\phi\rho_s\varepsilon_s v_{s,slip}^2 g_0\theta^{\frac{3}{2}}}{6\varepsilon_{s,max}\gamma_W} \quad (5)$$

where $\gamma_W=\frac{\sqrt{3}\pi\left(1-e_W^2\right)\varepsilon_s\rho_s g_0\theta^{3/2}}{4\varepsilon_{s,max}}$.

Results

Riser-sorber

Hydrodynamics Behavior. The computed transient distributions of solid volume fraction and solid velocity magnitude vectors at different flow times inside the riser-sorber are shown in Figures 7 and 8, respectively. The results show that there are a lot of fluctuations in the solid-volume fraction, giving riser a good mixing. However, the variation in the distribution of the solid-volume fraction is not very large. Quantitatively, mixing is described by radial and axial dispersion coefficients or by the granular temperature of the

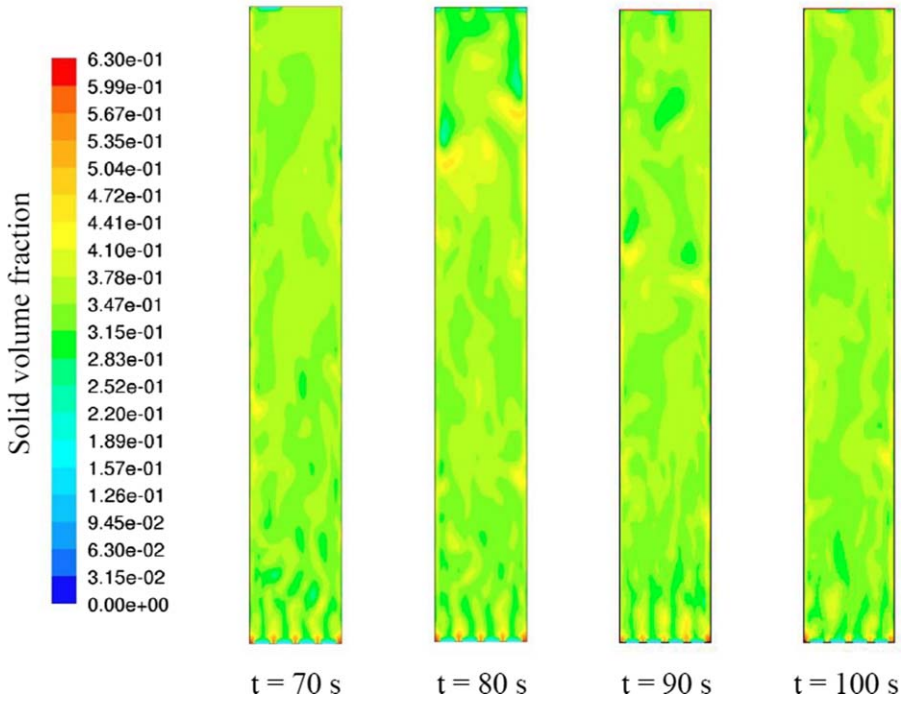

Figure 7. Computed solid volume fraction in fluidized-bed riser.

[Color figure can be viewed in the online issue, which is available at wileyonlinelibrary.com.]

particles. The granular temperature is the average variance of the particle velocity distribution. The total granular temperature for the riser-sorber is shown by the green star in Figure 9. This figure is that given in the article by Chalermsinsuwan et al.[14] with the addition of the simulation done in this study. It shows that our computed granular temperature is close to the experimental data for 500 micron particles. To demonstrate symmetric profiles and low variation in solid-volume fraction, time-averaged solid sorbent volume fraction axial distributions in the riser section at three locations; right wall, center and left wall (0.25 m, 0.5 m, and 0.75 m from the left wall) are plotted in Figure 10. The time-averaging of the solid-volume fractions was done over 50 s of flow time after the system reached a quasi-steady-state. The profiles show that the regions at the left side, center, and right side have nearly the same solid-volume fraction in the riser. There are only small variations near the inlet and outlet area due to entrance and exit effects.

Figures 11a,b and 12a,b show the radial distributions of solid sorbent volume fractions, axial pressure profile at the center of the riser-sorber, and the time-averaged axial velocities of the solid sorbent and the gas at riser levels of 2.0, 4.0 and 6.0 m from the bottom, respectively. These three different heights are selected to represent the bottom, center and top of the riser-sorber. The time-averaged solid-volume fraction and solid axial velocity were done over 50 s of flow time after the system reached the quasi-steady-state. The radial distribution of solid-volume fraction is mostly flat

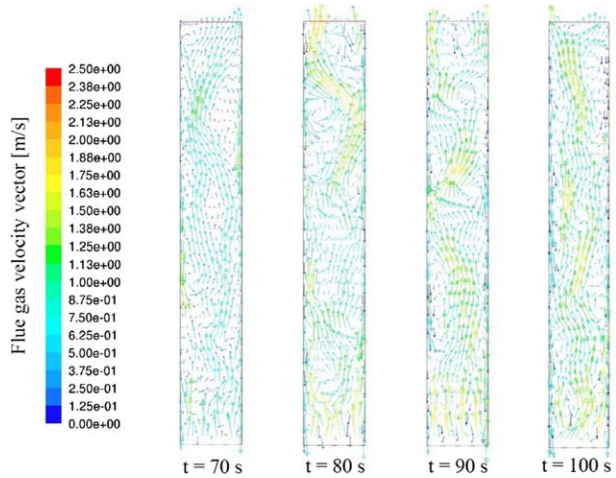

Figure 8. Computed flue-gas velocity vector in fluidized-bed riser.

[Color figure can be viewed in the online issue, which is available at wileyonlinelibrary.com.]

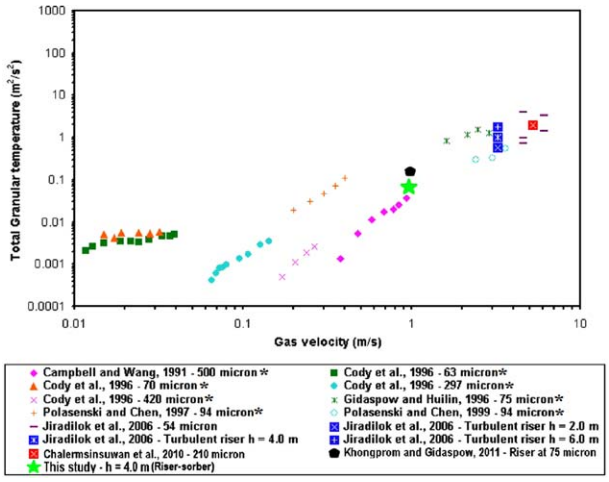

Figure 9. Comparison of experimental and computed total granular temperatures.

[Color figure can be viewed in the online issue, which is available at wileyonlinelibrary.com.]

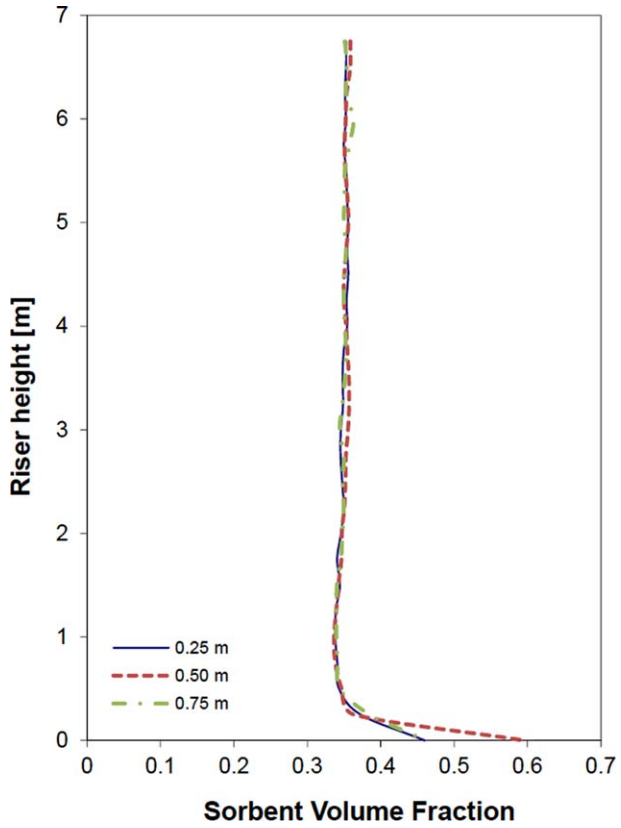

Figure 10. Time-averaged solid-volume fraction axial distributions at 0.25 m, 0.50 m (center line), and 0.75 m of riser-sorber.

[Color figure can be viewed in the online issue, which is available at wileyonlinelibrary.com.]

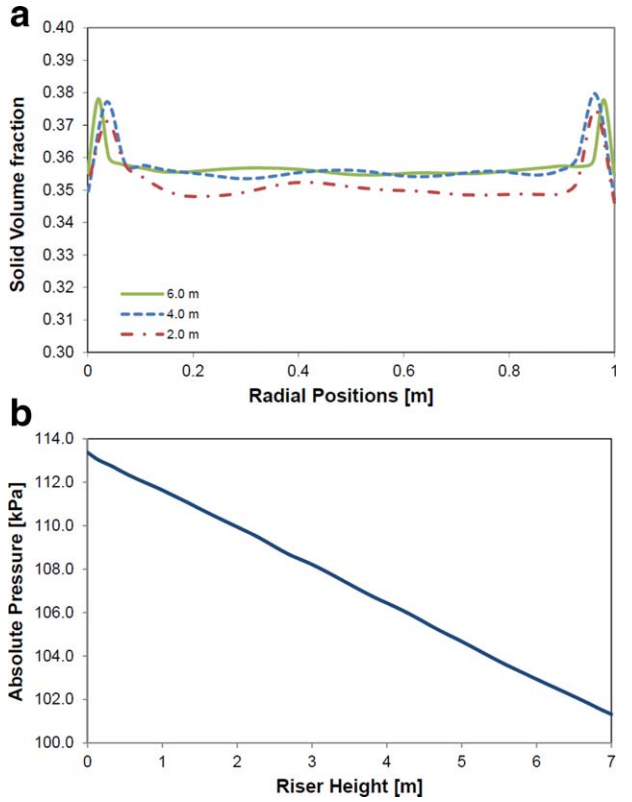

Figure 11. (a) Time-averaged solid sorbent volume fractions for the riser-sorber. (b) Axial pressure profile at the riser-sorber center line.

[Color figure can be viewed in the online issue, which is available at wileyonlinelibrary.com.]

across the riser-sorber except in the regions near the wall which show slightly higher solid-volume fractions than the other regions. The calculated solid-volume fraction from the axial pressure profile shown in Figure 11b is approximately 0.35, which agrees with the solid volume fraction profile shown in Figure 11a

$$\varepsilon_s = \frac{\Delta P}{\rho_s g L} = \frac{(113.4–101.3)\,[\mathrm{kPa}]}{500[\mathrm{kg/m^3}]\times 9.81[\mathrm{m/s^2}]\times 7[\mathrm{m}]} = 0.351 \qquad (6)$$

A video of particle concentration as a function of time showed periodic rising cluster formation next to the walls. The clusters disappeared next to the outlet. Similarly, the time-averaged solid axial velocity profile is relatively flat across the riser-sorber except near wall regions at all three different levels. Negative solid axial velocities near the wall regions showed that there is a downflow of the solid sorbent. Figures 11a and 12a imply that only a small amount of solid sorbent is flowing downward in the wall regions. The downflow of solid sorbent is an indication of the back-mixing inside the system which increases the opportunity for solid sorbent to react. However, this flow behavior also has a disadvantage because it will make the rate of CO_2 removal to be heterogeneous in the radial direction. Eliminating the core-annular regime helps to reduce the channeling of the fluegas which causes CO_2 to break-through. The gas profile without the core-annular regime represents better mixing. Hence, a shorter column can be used to achieve the same CO_2 removal. It is known that it is undesirable to have a core-annular flow in the riser-sorber. Comparing the simulation results for the riser and the CFB, which has a solid sorbent feed from the side and the flue feed from the bottom, as done by Chalermsinsuwan et al.[14] we see that the core-annular flow structure can be almost eliminated by feeding the flue gas and the solid sorbent into the system through multiple jet inlets.

The granular temperature is the average variance of the particle velocity distribution. Figure 13 shows the radial distributions of computed time-averaged total granular temperature in the riser-sorber at 2, 4, and 6 m heights. The figure shows that the time-averaged solid granular temperature is higher near the wall region and stays flat across the riser column. This behavior is similar to that for turbulent normal stresses in single phase turbulent flow. The turbulent intensity is defined as square-root of the granular temperature divided by the solid velocity. From Figures 12a and 13 the turbulent intensity is approximately 0.61 at the center of the riser compared to the theoretical value of 0.5 for a dilute riser flow.[34]

Carbon Dioxide Sorption. The simulation results for the carbon dioxide removal performance of the riser-sorber are shown in Figures 14 and 15. Figure 14 shows the transient computed mole fractions of CO_2 in the riser-sorber at 70, 80, 90, and 100 s of flow time. Figure 15 shows the time-averaged computed mole fraction of CO_2 and the percent CO_2 removal along the centerline of the riser-sorber. Figure 15 shows that most of the CO_2 sorption reaction occurs in the first 4 m of the riser-sorber. This is due to the fact that reaction rate is proportional of the CO_2 and H_2O molar

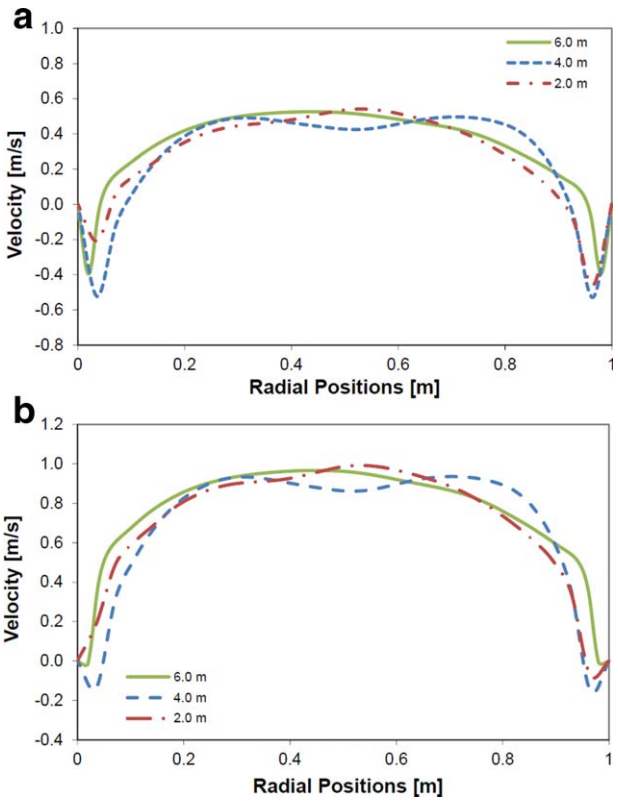

Figure 12. (a) Time-averaged solid axial velocity in the riser-sorber. (b) Time-averaged gas axial velocity in the riser-sorber.

[Color figure can be viewed in the online issue, which is available at wileyonlinelibrary.com.]

concentration gradient between actual and equilibrium conditions, which both decrease exponentially with riser-sorber height. The CO_2 gradient becomes near zero at the outlet where the equilibrium mole fraction of the CO_2 is approximately 0.06 and the $CO_{2\ mol}$ fraction at the outlet is approximately 0.07. The proposed that reaction rate is a second-order reaction rate. Therefore, the fast CO_2 sorption is predicted to occur in the bottom section of the riser-sorber. The simulation results show that approximately 60% of CO_2 can be removed from the flue gas using a 7 m riser-sorber. The outlet mole fractions of CO_2 and H_2O are about 7.5%. Due to the nearly flat solid axial

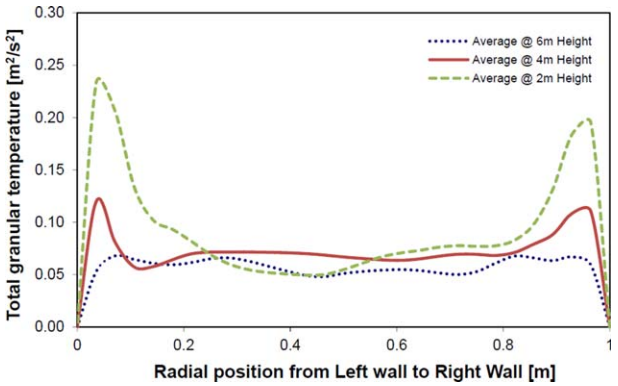

Figure 13. Radial distributions of computed time-averaged total granular temperature in the riser-sorber at different heights.

[Color figure can be viewed in the online issue, which is available at wileyonlinelibrary.com.]

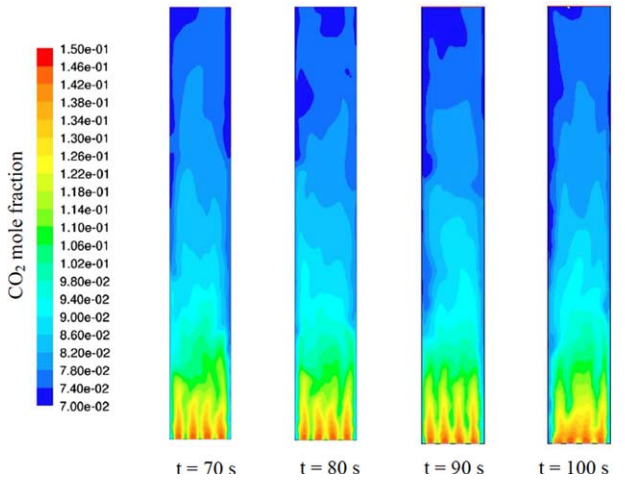

Figure 14. Computed mole fraction of CO_2 in fluidized-bed riser.

[Color figure can be viewed in the online issue, which is available at wileyonlinelibrary.com.]

velocity and solid volume fraction profiles in radial distribution, the CO_2 sorption variation is very small except near the wall region. In pyropower type circulating fluidized bed (CFB) of Chalermsinsuwan et al.[14] the absorption in the center of the riser is poor due to the core-annular flow regime. With the current riser-sorber height, operating conditions, and the use of 500 micron sorbent particles, a 90% of CO_2 removal cannot be achieved. Hence, it is proposed that a second riser-sorber column be used. The alternatives are to improve the CO_2 sorption rate or to use solid sorbents, such as lithium carbonate.

Figure 16 shows the computed solid sorbent temperatures for transients at 70, 80, 90 and 100 s of flow time. The inlet temperature is 62°C and the outlet temperature is 65°C. This small temperature rise is due to the high-solid circulation rate as already shown by Chalermsinsuwan et al.[14] The energy released from the CO_2 sorption reaction is absorbed by the solid sorbent as sensible heat. The energy captured in the solid sorbent is later on used in the downer-regenerator as the supplementary energy for the desorption reaction. Figure 17 shows the sorbent temperature profiles in the axial direction at three different distances from the left wall of the riser-sorber. The time-averaged solid temperature profiles are averaged over 50 s of flow time after the system reached a

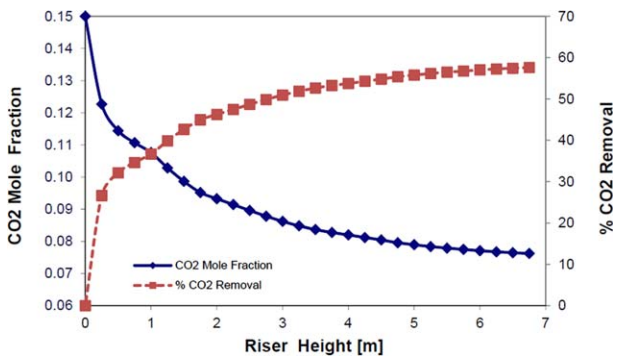

Figure 15. Time-averaged mole fraction of CO_2 and percent CO_2 removal during sorption at the center line of riser-sorber.

[Color figure can be viewed in the online issue, which is available at wileyonlinelibrary.com.]

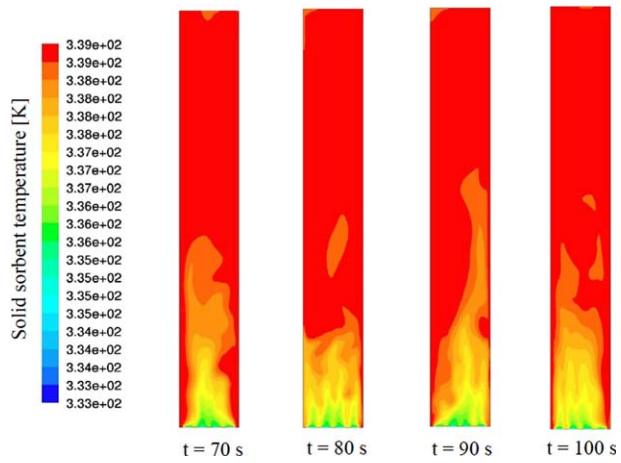

Figure 16. Computed solid sorbent temperature in fluidized-bed riser.

[Color figure can be viewed in the online issue, which is available at wileyonlinelibrary.com.]

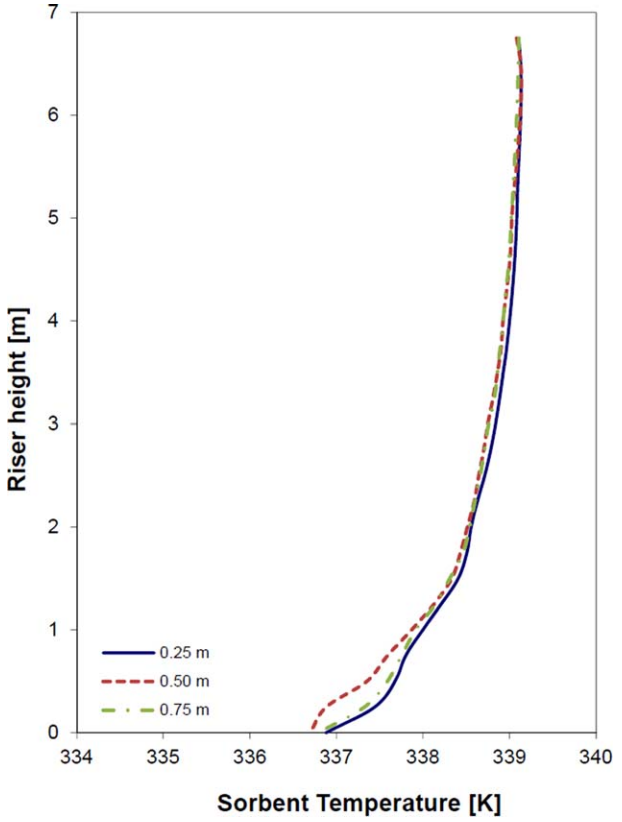

Figure 17. Time-averaged solid temperature axial distributions at 0.25 m, 0.50 m (center line), and 0.75 m of riser-sorber.

[Color figure can be viewed in the online issue, which is available at wileyonlinelibrary.com.]

quasi-steady-state. The figure shows that the solid temperatures along the left, center, and right sections have nearly the same profile. There are only small variations near the inlet and outlet area due to entrance effect. This is due to the hydrodynamics inside the riser-sorber where there is almost no core-annular flow regime. The solid temperature sharply increased from the bottom to the 4 m height. Above 4 m in height, the solid temperature profiles stay almost unchanged. This is due to the fact that CO_2 sorption reaction occurred mostly in the first 4 m of the riser-sorber height. In this simulation, we assumed the wall to be adiabatic.

Downer-regenerator

Hydrodynamics Behavior. The computed transient distributions of solid volume fraction and solid velocity magnitude vectors at different flow times inside the downer-regenerator are shown in Figures 18 and 19, respectively. Figure 18 shows that the solid-volume fraction in the downer-regenerator is divided into two main regions: the dense region and the dilute region. The dense region is mainly at the bottom of the downer while the dilute region occurred mostly near and/or above the inlet feed slot. The simulation results showed that there are a lot of fluctuations in the solid-volume fraction in the downer-regenerator.

The simulation result showed that the solid sorbents, which dropped to the bottom of the downer-regenerator by gravity, have a higher fluctuation of the volume fraction compared to the riser-sorber. This is due to desorption of gases, mainly CO_2 and water vapor, from the solid sorbent

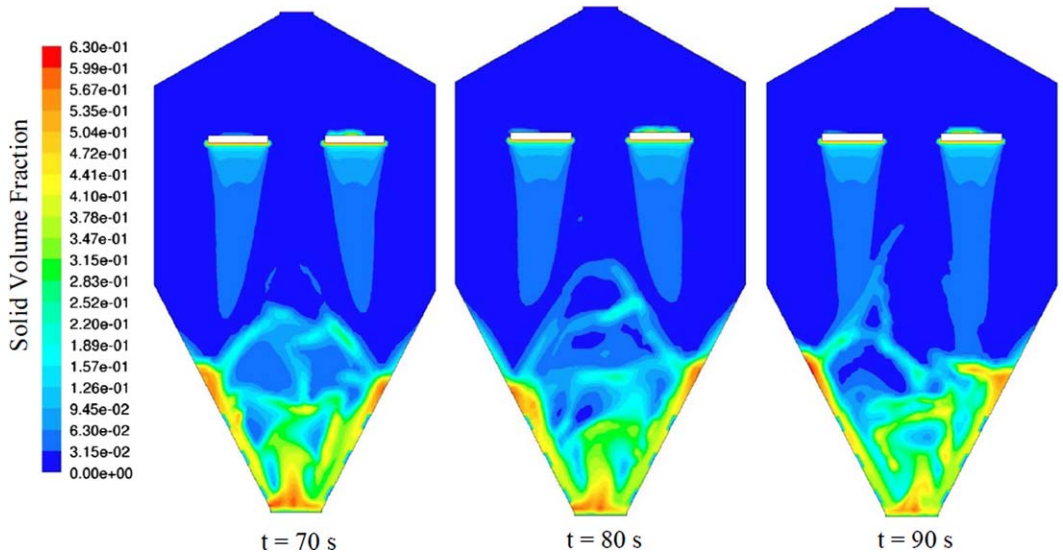

Figure 18. Computed solid sorbent volume fraction in downer-regenerator.

[Color figure can be viewed in the online issue, which is available at wileyonlinelibrary.com.]

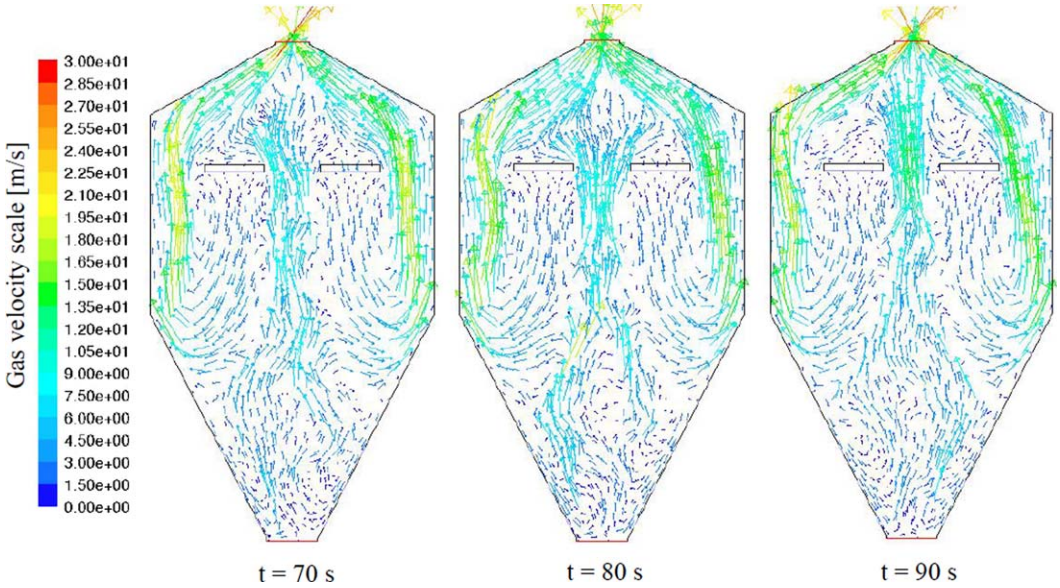

Figure 19. Computed Gas velocity vector in downer-regenerator.

[Color figure can be viewed in the online issue, which is available at wileyonlinelibrary.com.]

under the vacuum pressure inside the downer-regenerator. The volume expansion of the desorbed gases under the vacuum pressure is much higher than the volume of gases sorbed in the riser-sorber. The higher expansion of the gases led to higher gas velocities inside the downer-regenerator. Therefore, the solid sorbent volume fluctuation in the downer-regenerator is much higher than the fluctuations in the riser-sorber. Figure 19 shows that the gas velocity vector near the bottom of the downer-regenerator is lower than in the upper region of the vessel. However, it is also noticeable that the gas velocity vector shows higher fluctuations in the bottom region inside downer-regenerator than in the other regions.

Figure 20 shows the time-averaged axial distributions of solid sorbent volume fraction in the downer-regenerator at the center of left feed and right feed inlets, as well as at the center of the downer. Due to the taper shape of the bottom section of the downer, the plots for left and right sections end at the vessel wall, this is approximately 0.5 m from the bottom of the vessel. Although the overall downer-regenerator height is 3.5 m, the figure shows only the solid volume fraction from the bottom of the downer up to the inlet feed slot height, which is at 2.6 m in height. This is due to the fact that the solid volume fraction approached zero at the inlet feed slots and remained near zero throughout the remainder of the space above the inlet slots. At the 2.6 m elevation, at the inlet slots height, the time-averaged solid-volume fraction in the left and right sections is nearly at the maximum solid packing density because the solid, fed by gravity into the downer-regenerator inlet slots via a lock-hopper rotary valve, is assumed to be at the maximum solid packing density. The figure shows that the solid sorbent accumulated mainly at the bottom of the downer, near the solid sorbent outlet. There is almost no solid sorbent presents in the region above the inlet feed slot. The solid-volume fraction in the left and right sections at 1.0 m elevation had higher fluctuations than at the normal elevation. Figure 21 shows the time-averaged radial distributions of solid sorbent volume fraction in the downer-regenerator at 0.25, 0.50 and 1.0 m elevations from the bottom of the vessel. The time-averaged solid-volume fractions in both Figures 20 and 21 are done over 60 s of flow time. Figure 21 showed the high solid-volume fractions near both left and right wall regions, while the central region was much more dilute. Figure 22 shows the time-averaged solid axial velocity from the left

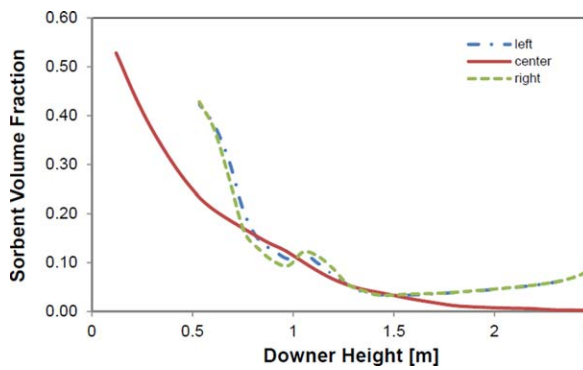

Figure 20. Time-averaged solid volume fraction in the axial direction in the downer-regenerator.

[Color figure can be viewed in the online issue, which is available at wileyonlinelibrary.com.]

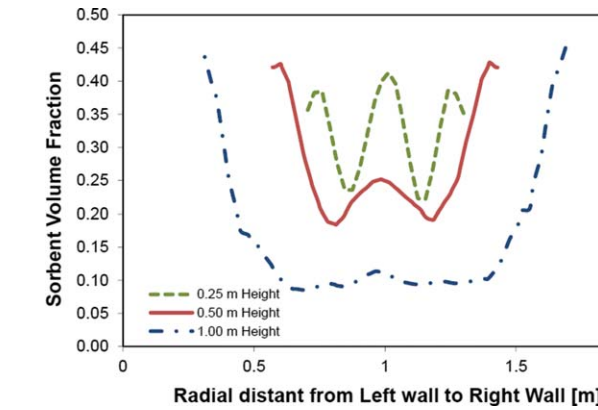

Figure 21. Time-averaged radial distribution of solid volume fraction at different elevations in the downer-regenerator.

[Color figure can be viewed in the online issue, which is available at wileyonlinelibrary.com.]

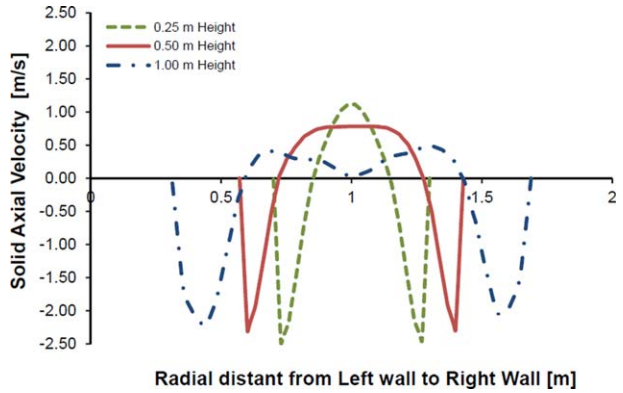

Figure 22. Time-averaged axial solid velocity at different elevations in the downer-regenerator.

[Color figure can be viewed in the online issue, which is available at wileyonlinelibrary.com.]

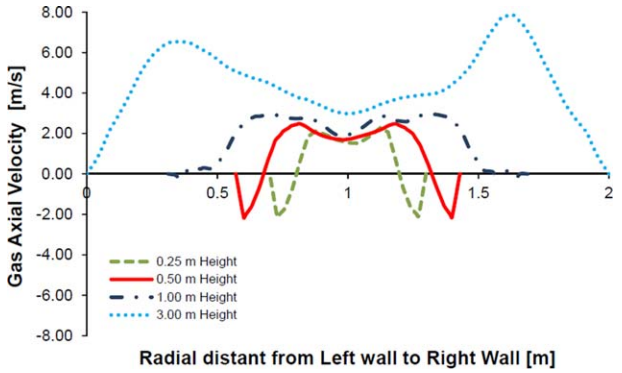

Figure 23. Time-averaged axial gas velocity at different elevations in the downer-regenerator.

[Color figure can be viewed in the online issue, which is available at wileyonlinelibrary.com.]

wall to the right wall at different elevations. It can be concluded that solid sorbent near the wall was pushed to the wall and flowed downward, while the solid sorbent near the center region flowed upward. Therefore, a core-annular flow regime is observed at the bottom of the downer-regenerator. Unlike the negative effect of a core-annular regime in the riser-sorber, having core-annular regime in the downer has no negative effect on the downer-regenerator performance. The core annular regime will provide more residence time for $NaHCO_3$ solid sorbent to reside, which will increase the residence time of the solid sorbent inside the downer-regenerator.

The downer-regenerator was chosen to have a unique shape and configuration, different from the riser-sorber. This unique configuration has a large middle section, which tapers down to the top and bottom outlet of the downer. The large middle section served three main purposes to ensure that the downer-regenerator operated properly. The first purpose is to minimize the pressure drop inside the downer. The second purpose is to ensure a low-gas velocity throughout the downer. Since the desorbed gas volume is large, due to the high-volume expansion into the vacuum pressure, the large middle area of the downer allows the gas velocity to reduce. Therefore, the solid sorbents are not blown away with the gases. The last purpose of having a large middle section is to allow the tapered wall from the middle section down to the outlet to have smooth flow of solid sorbent down to the outlet area, without any dead spots.

Figure 23 shows the time-averaged gas axial velocity from left wall to right wall at different elevations. The gas axial velocity is observed to have a similar trend to the solid axial velocity. However, there is a slip velocity between the two phases due to the density difference. The gas phase has a higher velocity than the solid sorbent phase. Gas and solid axial velocity profiles, as well as the solid-volume fraction profiles show a strong symmetry consistently through multiple elevations in the downer-regenerator.

Solid Sorbent Regeneration. The simulation shows a good performance and capability of solid sorbent regeneration inside the downer-regenerator operated under reduced pressure. The desorbed gases from $NaHCO_3$ solid sorbent consist mainly of CO_2 and water vapor. Once desorption process is done, the $NaHCO_3$ converted back to Na_2CO_3 which is recycled back into the riser-sorber. Figure 24 shows the computed mole fraction of sodium bicarbonate ($NaHCO_3$) inside the downer-regenerator for transients at 70,

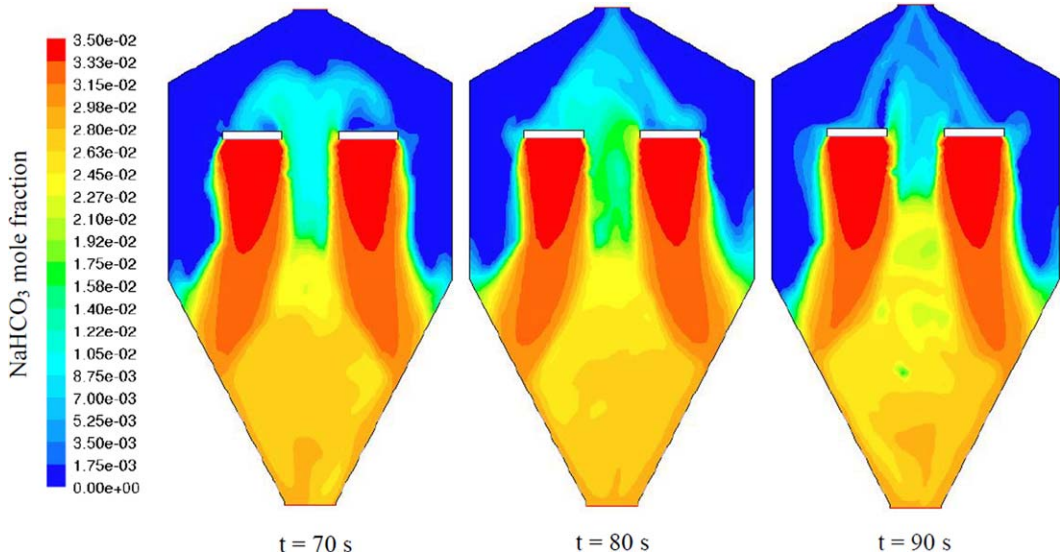

Figure 24. Computed mole fraction of $NaHCO_3$ in downer.

[Color figure can be viewed in the online issue, which is available at wileyonlinelibrary.com.]

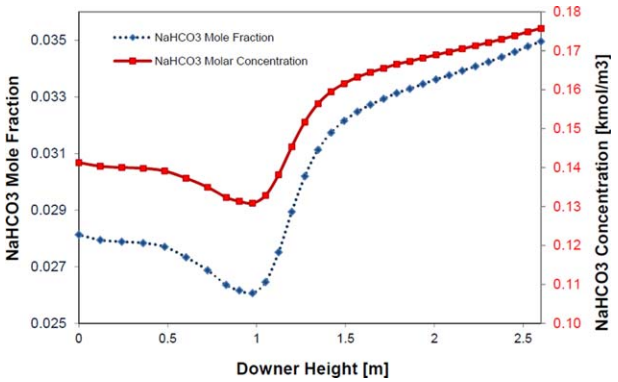

Figure 25. Time-averaged $NaHCO_3$ concentration and mole fraction during desorption at the center line of reduced pressure downer-regenerator.

[Color figure can be viewed in the online issue, which is available at wileyonlinelibrary.com.]

80 and 90 s of flow time. The mole fraction of $NaHCO_3$ is high at the feed inlet slot, and then it is gradually reduced when the solid is falling down to the bottom of the downer. Due to the high mixing in the bottom zone inside the downer, the mole fraction of $NaHCO_3$ stays mostly uniform, except at the wall region where the gas and solid velocities are low. Figure 25 shows the time-averaged computed mole fraction and concentration of $NaHCO_3$ along the centerline of the downer-regenerator, from feed inlet elevation to the bottom outlet.

The figure shows that the $NaHCO_3$ concentration is linearly reduced along the downer height from 2.6 m to 1.5 m. Then the $NaHCO_3$ concentration drops sharply at the downer height between 1.5 m and 1.0 m. From the 1.0 m height down, the $NaHCO_3$ concentration increases gradually and later are stable around 0.5 m height. This phenomenon can be explained due to the fact that the equilibrium pressures of CO_2 and water vapor change exponentially with the temperature. Figure 2 shows that the equilibrium pressure of CO_2 and water vapor exponentially increases once the temperature dropped. The temperature inside the downer decreases because the desorption reaction is endothermic. Therefore, the CO_2 and H_2O molar concentration gradient between actual and equilibrium conditions increases sharply. As a result, the desorption rate exponentially increased. However, because of the high solid-volume fraction in the lower regions of the downer near the bottom outlet, the operating pressure near the bottom is higher. This causes the CO_2 and H_2O molar concentration gradient to shift, which leads to the increasing of $NaHCO_3$ concentration in the bottom region.

Figure 28 shows the computed time-averaged solid sorbent temperature profiles in axial direction at three different distances from the left wall. The time-averaged solid temperature profiles are done over 60 s of flow time after the system reached a quasi-steady-state. The left and right sections start at 2.6 m height, where the inlet feed slots are located. Along the left and right sections, the inlet solid temperature is 65.5°C. It drops along the downer height to 62.5°C, once it reaches the downer wall. The temperature drop is anticipated since the desorption reaction is the endothermic. This small temperature drop at the bottom region is due to the energy released from the solid sorbents used in the regeneration process. In the bottom region, the solid temperature at the centerline stays nearly constant since the desorption reaction reached the equilibrium and the mixing is high. The solid temperature along the centerline above 1.5 m height to the top outlet shows a linear reduction in the temperature. This is due to the gas expansion under the vacuum pressure in the overhead area where the solid volume fraction is very low. The gas expansion causes both gas and solid temperatures to drop. The simulations show that the reduced pressure downer-regenerator of a height of 3.5 m and a width of 2.0 m can be operated successfully in a cyclic manner with a 7.0 m tall and 1.0 m wide riser-srober.

Thermodynamics and availability

Figures 29 and 30 show the availability and entropy cycle for the complete riser-sorber and downer-regenerator loop system. Both the entropy and the availability increase during the CO_2 sorption step in the riser-sorber. On the other hand, both the entropy and the availability decrease during the CO_2 desorption step in the downer-regenerator. The increasing entropy and availability inside riser-sorber is mainly due to the increase in gas and solid temperatures. Higher temperature means higher entropy and availability. The change in the gas and solid composition also contribute to the change in entropy and availability; however, for this particular riser-downer system, changes in gas and solid a composition show considerably smaller impact to the entropy and availability than the temperature change. On the other hand, the entropy and availability decreases in the downer-regenerator (from the inlet to outlet condition) due to the work input from the vacuum fan. The vacuum pressure causes desorption reaction inside the downer-regenerator; as a result, the gas and solid temperatures are lower. The lower temperatures cause the entropy and the availability to decrease. However, the overall entropy of the system still increases. Only the subsystem (gas–solid mixture only) entropy can go down due the reduction in temperature of the gas–solid mixture. Similarly, the entropy and availability reduction occurred when the solid sorbent moved from the downer-regenerator to the riser-sorber because the air-lock rotary valve that transports the solid sorbent from the downer to the riser required a work input.

The basic of availability balance equation for a flow system shown in Figure 31 can be written as

$$\frac{d(m(U-T_0S))_{\text{system}}}{dt}=\left(\sum_{i=1}^{n}\dot{m}_i(h_i-T_0S_i)-\sum_{i=1}^{n}\dot{m}_o(h_o-T_0S_o)\right)+\sum_{j=1}^{m}\left(1-\frac{T_0}{T_j}\right)\dot{Q}_j-\dot{W}-T_0\sigma \tag{7}$$

$$\begin{array}{ccccccccc}\text{rate of accumulation of Helmholtz type availability} & = & \text{net rate of availability inflow due to the mass inflow} & + & \text{availability of heat inflow} & - & \text{Rate of work} & - & \text{Rate of availability consumption}\end{array}$$

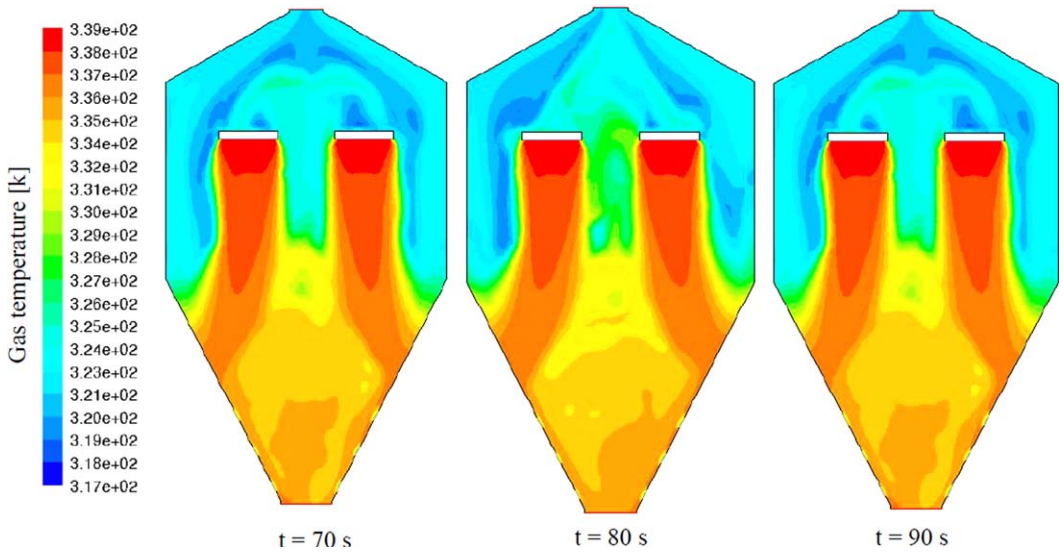

Figure 26. Computed gas temperature in downer-regenerator.

[Color figure can be viewed in the online issue, which is available at wileyonlinelibrary.com.]

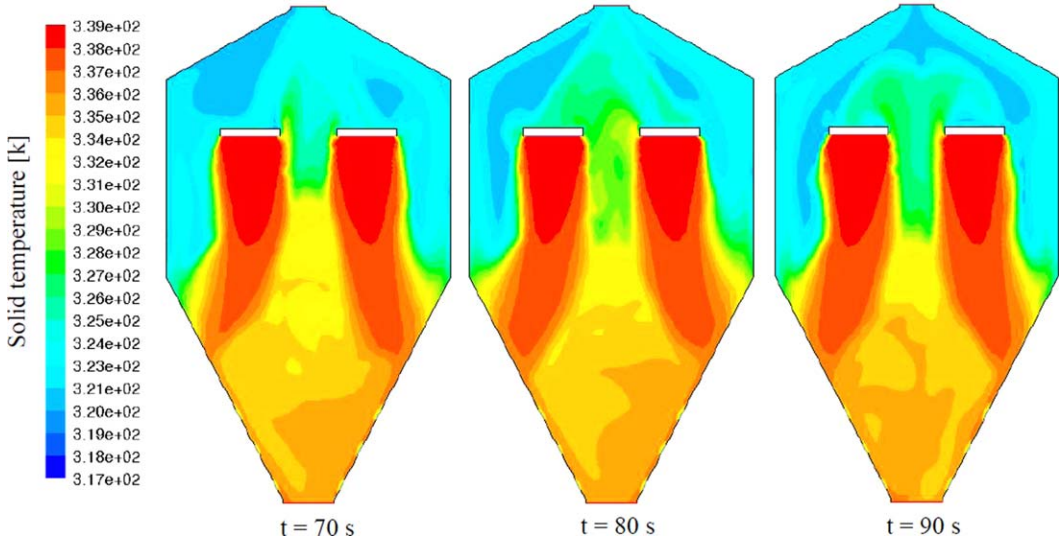

Figure 27. Computed solid sorbent temperature in downer-regenerator.

[Color figure can be viewed in the online issue, which is available at wileyonlinelibrary.com.]

Table 4. Computed Overall Availability on the Riser-Sorber and Downer-Regenerator[38]

Availability for the riser-sorber					
Quantities		Riser Inlet	Riser Outlet	Blower	Riser Overall
Availability	[kJ/s]	112.59	−133.60	7.26	−13.75
Availability/Weight	[J/gCO2]	1464.51	−1737.76	94.37	−178.89
Availability/mole	[kJ/gmolCO2]	**64.44**	**−76.48**	**4.15**	**−7.87**

Availability for the downer-regenerator					
Quantities		Downer Inlet	Downer Outlet	Vacuum fan	Downer Overall
Availability	[kJ/s]	131.69	−109.31	38.69	61.06
Availability/Weight	[J/gCO2]	1808.03	−1500.83	531.17	838.37
Availability/mole	[kJ/gmolCO2]	**79.55**	**−66.05**	**23.37**	**36.89**

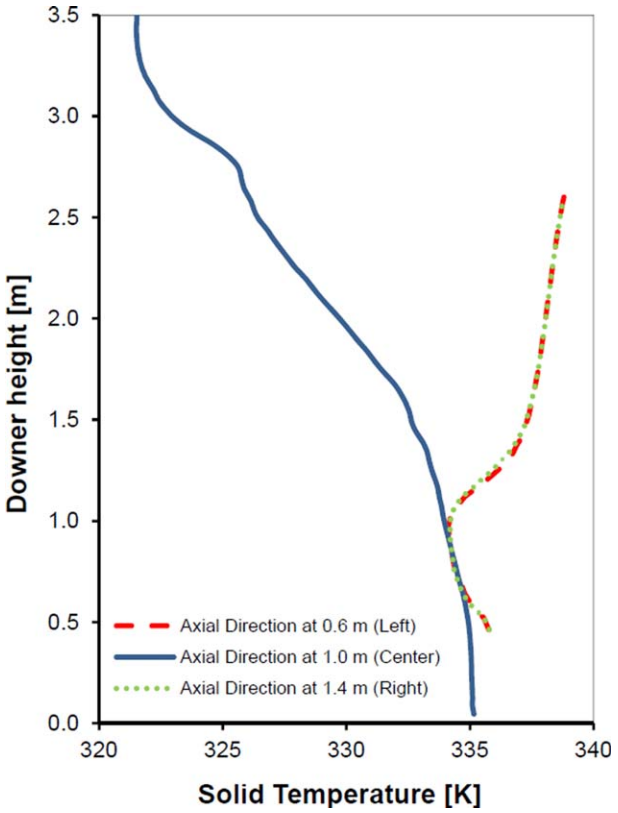

Figure 28. Time-averaged solid temperature axial distributions at 0.6 m, 1.0 m (center line), and 1.4 m from the downer left wall.

The left and right axial start from the solid inlet feed slot and end at the downer vessel wall. [Color figure can be viewed in the online issue, which is available at wileyonlinelibrary.com.]

The availability balance for the riser at adiabatic operation, a steady state and no work done on the riser other than inlet gas blower can be reduced from a standard steady-state availability balance down to the equation as follows

$$T_0\sigma=\sum_{i=1}^{n}\dot{m}_i(h_i-T_0S_i)-\sum_{i=1}^{n}\dot{m}_o(h_o-T_0S_o)-\dot{W}_{\text{Blower}} \quad (8)$$

Similarly, the rate of loss of availability (irreversibility) on the downer-regenerator with the assumption of adiabatic, steady state and no work done on the downer other than that for the outlet gas vacuum fan can be calculated from the availability balance as shown below

$$T_0\sigma=\sum_{i=1}^{n}\dot{m}_i(h_i-T_0S_i)-\sum_{i=1}^{n}\dot{m}_o(h_o-T_0S_o)-\dot{W}_{\text{Vacuum}\,fan} \quad (9)$$

The availability balance for overall system is used to determine the minimum energy required to remove the CO_2 from the flue gas using the dry sorbent riser-downer loop system. By combining the availability balance equation for the riser-sorber and downer-regenerator, the overall rate of loss of availability (required energy of separation) can be written as shown in the following

$$T_0\sigma|_{\text{Total}}=\left[\sum_{i=1}^{n}\dot{m}_i(h_i-T_0S_i)-\sum_{i=1}^{n}\dot{m}_o(h_o-T_0S_o)\right]_{\text{Riser}}+\left[\sum_{i=1}^{n}\dot{m}_i(h_i-T_0S_i)-\sum_{i=1}^{n}\dot{m}_o(h_o-T_0S_o)\right]_{\text{Downer}}-\dot{W}_{\text{blower}}-\dot{W}_{\text{Vacuum\_fan}} \quad (10)$$

An estimate of the theoretical minimum power consumption for the blower or vacuum fan can be calculated from basic thermodynamics relationships. We make two assumptions (1) idea gas law, and (2) isentropic operation

$$\dot{W}=\frac{\dot{m}\,C_pT_{\text{inlet}}}{\eta_{\text{Compressor}}}\left[\left(\frac{P_{\text{outlet}}}{P_{\text{inlet}}}\right)^{\left(\frac{\gamma-1}{\gamma}\right)}-1\right] \quad (11)$$

Table 4 shows the computed availability for the process at the inlet, outlet, for the blower/vacuum fan, and the overall riser-sorber and downer-regenerator availability. The overall availability loss of the entire sorber-regenerator loop system is 29.0 kJ/g mol-CO_2 which represents the total required energy input for the system. Most of the required energy input to the system comes from the inlet gas blower and vacuum fan. The work input for the flue gas blower is 4.1 kJ/g mol-CO_2 and 23.3 kJ/g mol-CO_2 for the vacuum fan which operated at 1 kPa(abs) suction pressure and atmospheric discharge pressure. The minimum required energy input can be

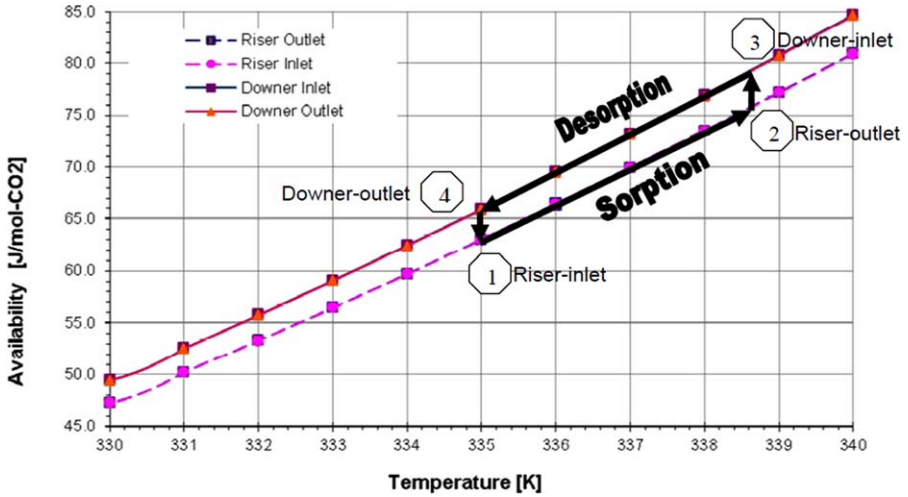

Figure 29. Availability for the riser-sorber and downer-regenerator CO_2 capture process.

[Color figure can be viewed in the online issue, which is available at wileyonlinelibrary.com.]

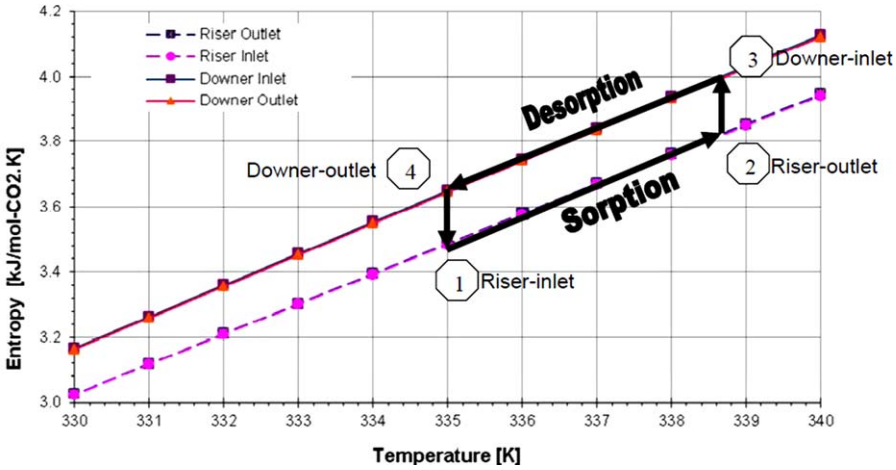

Figure 30. Entropy for the riser-sorber and downer-regenerator CO_2 capture process.

[Color figure can be viewed in the online issue, which is available at wileyonlinelibrary.com.]

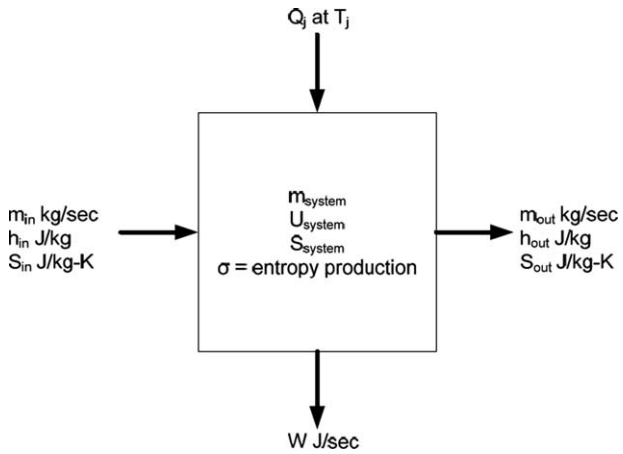

Figure 31. Flow system.

reduced significantly if the downer-regenerator can be operated at 5 kPa(abs). At 5 kPa(abs) suction pressure the energy consumption for the vacuum fan is reduced down to 12.2 kJ/g mol-CO_2. This leads to a 38% reduction of the overall energy consumption for the entire system. It is also noted that the overall availability increase across the riser-sorber is approximately 12.0 kJ/g mol-CO_2, while the overall reduction in availability in the downer-regenerator is approximately 13.5 kJ/g mol-CO_2. This implies that up to 88% of the heat liberated in the sorber is recovered in the downer regenerator. The loss in thermodynamic availability is only 1.5 kJ/g mol-CO_2.

To achieve a higher CO_2 removal, now limited by the equilibrium decomposition pressure of the carbonate, it is necessary to have a two-stage process with the second stage sorber-riser operating at lower temperature. The proposed process is shown in Figure 32. To reduce the vacuum fan energy consumption for the regenerator-downer, the conical walls of the regenerator-downer shown in Figure 18 can be heated using hot inlet flue gases.

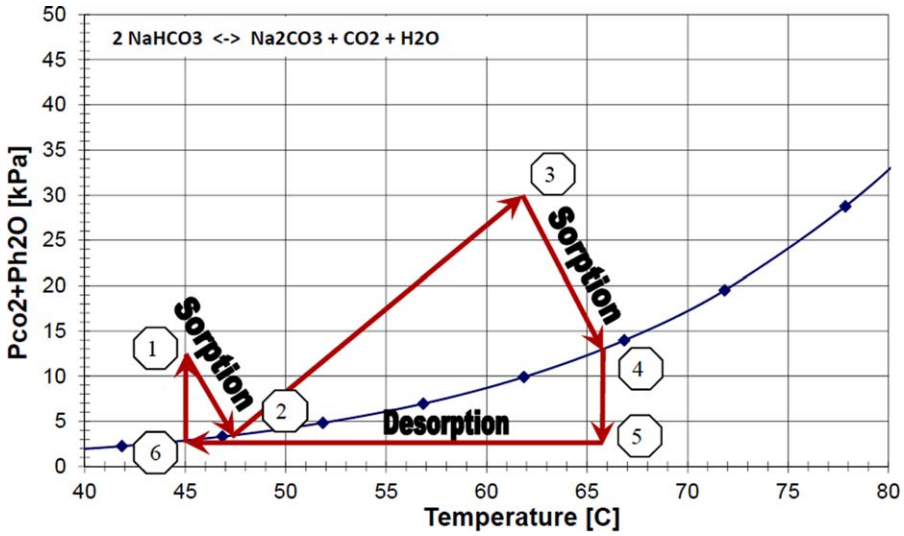

Figure 32. Proposed two stage process.

[Color figure can be viewed in the online issue, which is available at wileyonlinelibrary.com.]

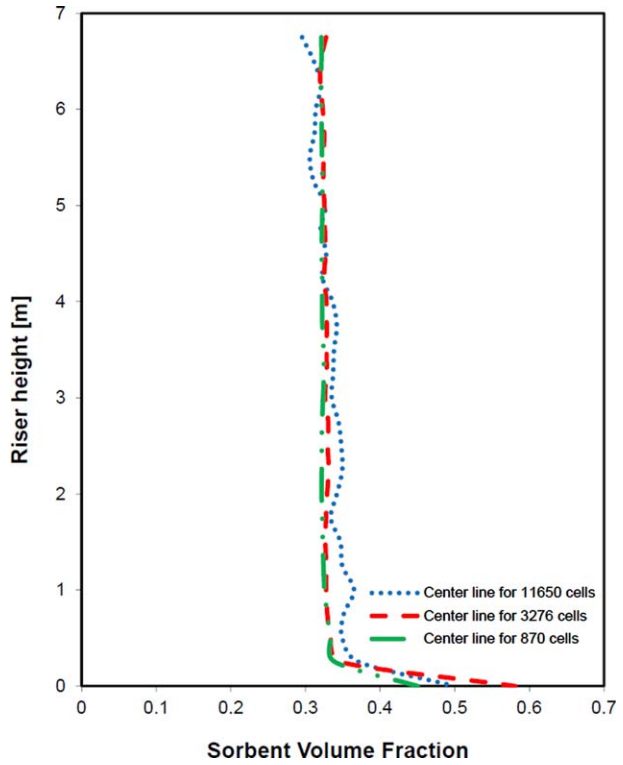

Figure 33. Computed time-averaged solid volume fraction at center of the riser-sorber in axial direction for three different numbers of cells.

[Color figure can be viewed in the online issue, which is available at wileyonlinelibrary.com.]

Grid Independence Study. The grid independence study is one of the important parts in numerical modeling. To prove that the simulation results are grid independent, the numbers of computational cells are varied for three levels; fine grid level, medium grid level, and coarse grid level. Ideally, the grid should be sufficiently fine so that further refinement does not change the result. The domains consist of 870, 3,276 and 11,650 computational cells in the riser-sorber. All the computational cells predict similar solid-sorbent-volume fraction profiles. Figure 33 shows the computed time-averaged solid-volume fractions at the center of the riser-sorber in the axial direction for three different numbers of cells. This indicates that all the grids are sufficiently fine for providing reliable results. The solid-volume fraction in the riser-sorber is approximately double that of computed by Kongporm and Gidaspow[21] for 75 micron particles at the same velocity of 1 m/s.

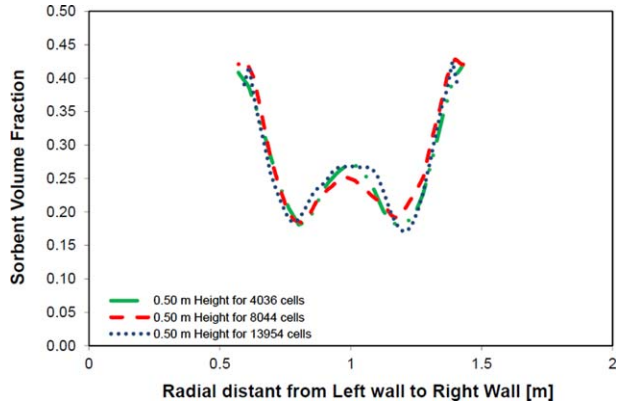

Figure 34. Computed time-averaged solid volume fraction in the downer-regenerator at 0.5 m height in radial direction for three different numbers of cells.

[Color figure can be viewed in the online issue, which is available at wileyonlinelibrary.com.]

Similarly, the grid independence study on the downer-regenerator was carried out. The downer-regenerator computational domains consist of 4,036, 8,044 and 13,954 computational cells. All the computational cells predict similar solid-sorbent-volume fraction profiles. Figure 34 shows computed time-averaged solid-volume fraction in the downer-regenerator at 0.5 m in height in the radial direction for three different numbers of cells. This indicates that all the grids are sufficiently fine for providing reliable results.

Conclusions

1. A fluidized-bed riser with a reduced pressure regeneration downer process was designed using multiphase CFD for removing CO_2 from flue gases. Approximately 60% of the CO_2 is removed in a 7 m high riser-sorber. To achieve a higher CO_2 removal, a second stage, a riser-sorber operating at a lower temperature is needed.
2. 500 micron sorbent particles were used rather than the 75 micron sorbent manufactured by RTI. The larger sorbent particle size allows better settling in the downer.
3. Using multiple jet inlets and the large sorbent particles, the undesirable core-annular regime in the riser is almost completely eliminated leading to a shorter height. The downer shows a core-annular regime flow pattern. However, there is no negative effect of having a core-annular flow regime inside the downer-regenerator.

Notation

c_p = heat capacity at constant pressure, J/kg K
d_p = particle diameter, m
e = restitution coefficient between particles
e_W = restitution coefficient between particle and wall
g = gravity force, m/s^2
g_0 = radial distribution function
G_s = solid sorbent circulation rate, kg/m^2 s
h = height of riser, m
h = heat-transfer coefficient J/s m K, or specific enthalpy, J/kg
H = enthalpy, J
ΔH = heat of reaction, MJ/kgmol
k = thermal conductivity, J/s m K
k_{reaction} = reaction rate constant, m^3/s kgmol
$\dot{m}$ = system mass flow rate, kg/s
M = metal of an alkaline
MW = molecular weight, kg/kgmol
n = unit vector or number of streams
P = gas pressure, Pa
$\dot{Q}$ = heat flow, MJ/s
Q_{gs} = intensity of heat exchange from gas phase to solid phase, J/s m^3
Q_{sg} = intensity of heat exchange from solid phase to gas phase, J/s m^3
r = reaction rate, kgmol/s m^3
R_j = reaction rate of specie j, kg/s m^3
S = source term (e.g., due to chemical reaction), J/s m^3
S = specific entropy, J/kg K
T = time, s
T = temperature, K
v = velocity, m/s

$\dot{W}$ = rate of work or power required, MJ/s
y_i = mass fraction of each species
Y = axial or vertical distance, m

Greek letters

β_{gs} = gas–solid interphase drag coefficient, kg/s m^3
ε = volume fraction
$\varepsilon_{s,\max}$ = solid-volume fraction at maximum packing
ϕ = specularity coefficient
γ = heat capacity ratio
γ_s = collisional dissipation of solid fluctuating energy, kg/m s^3
γ_W = collisional dissipation of solid fluctuating energy at the wall, kg/m s^3
κ_s = conductivity of the fluctuating energy, kg/m s
μ = viscosity, kg/m s
π = mathematical constant $\approx$ 3.14
ρ = density, kg/m^3
θ = granular temperature, m^2/s^2
θ_t = turbulent granular temperature, m^2/s^2
θ_W = granular temperature at the wall, m^2/s^2
τ = stress tensor, Pa
ω = effectiveness or coefficient of performance
ξ_s = bulk viscosity, kg/m s
σ = entropy generation rate, J/s K
η = efficiency factor
α = stoichiometric coefficient

Subscripts

CO_2 = carbon dioxide specie
g = gas phase
H_2O = water specie
i = i direction or Inlet
j = j specie
o = outlet
R = regeneration reaction
s = solid phase
S = sorption reaction
x = radial direction
y = axial direction
0 = initial condition or reference state

Literature Cited

1. U.S. Energy Information Administration. Office of Electricity, Renewables & Uranium Statistics. Electric Power Monthly. February, 2012.
2. Pennline HW, Luebke DR, Jones KL, Myers CR, Morsi BI, Heintz YJ, Ilconich JB. Progress in Carbon dioxide capture and separation research for gasification-based power generation point sources. *Fuel Process Technol*. 2008;89:897–907.
3. Ciferno JP, Plasynski SI. Advanced Carbon Dioxide Capture R&D Program: Technology Update. DOE/NETL September, 2010.
4. Zhen-shan L, Ning-sheng C, Croiset E. Process analysis of co2 capture from flue gas using carbonation/calcination cycles. *AIChE J*. 2008;54(7):1912–925.
5. Holt NA. Evaluation of Innovative Fossil Fuel Power Plants with CO_2 Removal. EPRI Interim Report to DOE NETL, December 2000.
6. Rochelle GT. Amine scrubbing for CO_2 capture. *Science*. 2009;325: 1652–654.
7. Jassim MS, Rochelle GT. Innovative absorber/stripper configurations for CO_2 capture by aqueous monoethanolamine. *Ind Eng Chem Res*. 2006;45(B):2465–472.
8. Chakma A. formulated solvents: new opportunities for energy efficient separation of acid gases. *Energy Sources*. 1999;21:51–62.
9. Oyenekan BA, Rochelle GT. Energy performance of stripper configurations for CO_2 capture by aqueous amines. *Ind Eng Chem Res*. 2006;45:2457–464.
10. Oyenekan BA. Modeling of Strippers for CO_2 Capture by Aqueous Amines [Ph.D. Thesis]. University of Texas at Austin, TX; 2007.
11. Nelson TO. Coleman JID, Green A, Gupta RP. The dry carbonate process: capture dioxide recovery from power plant flue gas. *Energy Procedia*. 2009;1:1305–311.
12. Nelson TO, Green DA, Box P, Gupta RP, Henningsen G, Turk BS. Carbon dioxide capture from flue gas using dry regenerable sorbents, Final report. DOE Cooperative Agreement No. DE-FC26-00NT40923, RTI International, January 2009.
13. Nelson TO, Box P, Green DA, Gupta RP. Carbon Dioxide Recovery from Power Plant Flue Gas Using Supported Carbonate Sorbents in a Thermal-swing Process. Proc. of Sixth Annual Conference on Carbon Capture and Sequestration, Pittsburgh, PA, May 7–20; 2007.
14. Chalermsinsuwan BP, Piumsomboon P, Gidaspow D. A computational fluid dynamics design of a carbon dioxide sorption circulating fluidized bed. *AIChE J*. 2010;56:2805–824.
15. Hayashi H, Furuyashiki N, Sugiyama S, Hirano S, Shigemoto N, Nonaka T. Efficient recovery of carbon dioxide from flue gases of coal-fired power plants by cyclic fixed-bed operations over K2CO3-on-carbon. *Ind Eng Chem Res*.1998;37:185–91.
16. Gidaspow D. Separation of gaseous mixtures by regenerative sorption on porous solids: Part I. In: Li NN, ed. A Fluid Porous Solid Reaction Model with Structural Changes. Recent Development in Separation Science. Boca Raton, FL: CRC Press; 1972;2:59–70.
17. Onischak M, Gidaspow D. Kinetics of the Reaction of CO_2 with Solid K2CO3. Proc. of 73rd National AIChE Meeting, Minneapolis, MN; 1972.
18. Gupta H, Fan LS. Carbonation-calcination cycle using high reactivity calcium oxide for carbon dioxide separation from flue gas. *Ind Eng Chem Res*. 2002;41:4035–042.
19. Lee SC, Kim JC. Dry Potassium-based Sorbents for CO_2 Capture. *Catal Surveys Asia*. 2007;11:171–85.
20. Chang-Keun Y, S-H Jo, Yongwon S, Lee J-B, Chong-Kul R. Continuous operation of the potassium-based dry sorbent CO_2 capture process with two fluidized-bed reactors. *Int J Greenhouse Gas Control*. 2007;1:31–36.
21. Kongporm P, Gidaspow D. Compact fluidized bed sorber for CO_2 capture. *Particuology*. 2010;8:531–535.
22. Gidaspow, D. Multiphase Flow and Fluidization: Continuum and Kinetic Theory Description. San Diego, CA: Academic Press; 1994.
23. Ding J, Gidaspow D. A bubbling fluidization model using kinetic theory of granular flow. *AIChE J*. 1990;36:523–38.
24. Tsuo YP, Gidaspow D. Computation of flow patterns in circulating fluidzed beds. *AIChE J*. 1990;36:885–96.
25. Onischak M, Gidaspow D. Separation of Gaseous Mixtures by Regenerative Sorption on Porous Solids: Part II. Regenerative Separation of CO_2. In: Li NN, ed. Recent Development in Separation Science. Boca Raton, FL: CRC Press; 1972;2:71–93.
26. Lee JB, Ryu CK, Baek J-I, Lee JH, Eom TH, Kim SH. Sodium-based dry regenerable sorbent for carbon dioxide capture from power plant flue gas. *Ind Eng Chem Res*. 2008;47:4465–472.
27. Templeton CC. Pressure-temperature relationship for decomposition of sodium bicarbonate from 200 to 600 F. *J Chem Eng Data*. 1978; 23(1):7–11.
28. Park SW, Sung DH, Choi BS, Lee JW, Kumazawa H. Carbonation kinetics of potassium carbonate by carbon dioxide. *J Ind Eng Chem*. 2006;12(4):522–30.
29. Yongwon S, Jo SH, Ryu H-J, Bae DH, Ryu CK, Yi C-K. Effect of water pretreatment on co2 capture using a potassium-based solid sorbent in a bubbling fluidized bed reactor. *Korean J Chem Eng*. 2007; 24(3):457–60.
30. Yongwon S, Jo S-H, Ryu CK, Yi C-K. Effects of water vapor pretreatment time and reaction temperature on CO(2) capture characteristics of a sodium-based solid sorbent in a bubbling fluidized-bed reactor. *Chemosphere*. 2007;69:712–18.
31. Mayank K, Gidaspow D. Measurements and computation of low mass transfer coefficients for fcc particles with ozone decomposition reaction. *AIChE J*. 2012;58:707–729.
32. Johnson PC, Jackson R. Frictional-collisional constitutive relations for granular materials, with application to plane shearing. *J Fluid Mech*. 1987;176:67–93.
33. Sinclair JL, Jackson R. Gas-particle flow in a vertical pipe with particle- particle interaction. *AIChE J*. 1989;35:1473–486.
34. Gidaspow D, Jung J, Singh RK. Hydrodynamics of fludization using kinetic theory: and emerging paradigm 2002 Flour-Daniel lecture. *Powder Technol*. 2004;148:123–141.
35. Yuanxiang W, Gidaspow D. Hydrodynamic simulation of methonal synthesis in gas-liquid slurry bubble column reactors. *Chem Eng Sci*. 2000;55:573–587.
36. Fluent, Inc. Fluent 6.2 User's Guide. Lebanon, Israel: Fluent, Inc.; 2005.
37. Gamwo IK, Gidaspow D, Jung J. Optimum catalyst size for slurry bubble column reactors. *Ind Eng Chem Res*. 2005;44: 6393–402.
38. Kongkitisupchai S. Carbon Dioxide Capture Using Solid Sorbents in a Fluidized Bed with Reduced Pressure Regeneration in a Downer [Thesis]. Chicago Il: Illinois Institute of Technology; 2012.

Manuscript received Aug. 22, 2012, and revision received Apr. 21, 2013.